

DEVELOPMENT OF A MASS DETECTION TECHNIQUE TO DETECT INTAKES OF RADIOACTIVE MATERIAL
AND THEIR RESULTING RADIATION EXPOSURES FOLLOWING A LARGE-SCALE RADIOLOGICAL RELEASE

A Dissertation

Presented to

The Faculty of the Nuclear Sciences and Engineering Program

Worcester Polytechnic Institute

Submitted in partial fulfillment

Of the Requirements for the Degree of

Doctor of Philosophy

By

Christopher B. Martel

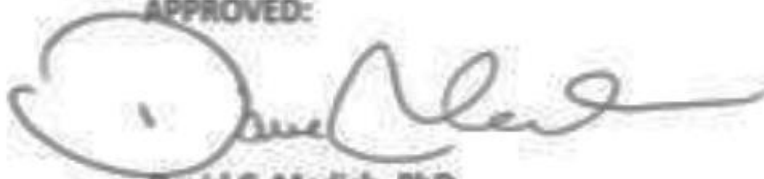
April 19, 2019

DEVELOPMENT OF A MASS DETECTION TECHNIQUE TO DETECT INTAKES OF RADIOACTIVE
MATERIAL AND THEIR RESULTING RADIATION EXPOSURES FOLLOWING A LARGE-SCALE
RADIOLOGICAL RELEASE

By

Christopher B. Martel

APPROVED:



David C. Medich, PhD

Thesis Director



Armin Ansari, PhD

Committee Member



Germano Iannacchione, PhD

Committee Member

DEDICATION

I dedicate this dissertation to my family. To my children, Jessica and Joshua, who are the best kids anyone could ever have. Their love, support and understanding has enriched my life more than I could have imagined. And to my wife Cindy, who sadly passed away unexpectedly on October 16, 2018. She was a source of incredible strength, wisdom and compassion to me, our children and to the many lives that she touched every day.

I love you all.

ABSTRACT

Martel, Christopher, *Development of a Mass Detection Technique to Detect Intakes of Radioactive Material and their Resulting Radiation Exposures Following a Large-Scale Radiological Release*. Medical Health Physics, May, 2019, Worcester Polytechnic Institute, Worcester, Massachusetts.

Large-scale radiological accidents have resulted in intakes of radioactive materials by members of the public and occupational radiation workers. However, current methods to evaluate intakes are designed for small numbers of individuals and cannot be easily scaled for large populations as has occurred. A proposed method for high throughput volumes of people to identify and quantify intakes of radioactive material through urine radiobioassay is described. MATERIALS AND METHODS: The MCNP V6.0 software code was used to model the General Electric Hawkeye V3 Gamma Camera for gamma ray efficiency. Technitium-99m was used to validate the model. The model was used to calculate detection efficiencies and minimum detectable doses for Cobalt-60, Iodine-131, Cesium-137/Barium-137m and Iridium-192. RESULTS: Differences of 8% were observed between measurements of the detection efficiency for Technitium-99m and the MCNP modeled detection efficiency (11.1% vs. 12.0%, respectively). Calculations showed that a dose of 20 mSv could be detected using urine radiobioassay in 6, 3, 2, and 20 days post incident for Type F intakes of Cobalt-60, Iodine-131, Cesium-137/Barium-137m and Iridium-192 respectively. Approximately 1,152 urine samples could be analyzed in an eight-hour shift using a single gamma camera. CONCLUSIONS: The use of the gamma camera for urine radiobioassay allows for high throughput volumes of samples and has sufficient detection sensitivity to meet dose-based decision guidelines.

KEY WORDS: Internal dosimetry, Intake of radionuclides, Cobalt-60, Iridium-192, Iodine-131, Cesium-137, Radiological accidents, Radiological terrorism, Gamma Camera

ACKNOWLEDGEMENTS

I would first like to acknowledge my advisor, Dr. David Medich, whose encouragement and persistent nagging kept me on the path to finishing my degree. And especially for his friendship and that of his wonderful wife Tara and adorable daughter Catharine, who made sure I ate my vegetables because I surely wasn't going to cook them for myself.

I also want to acknowledge the assistance and insightful questions from my colleagues Norbert Hugger and Andrew Daudelin. Thank you.

I would also like to thank the talented and wonderful medical staff at the Lahey Medical Center in Burlington, Massachusetts. In addition to providing me with unfettered access to equipment and personnel needed to conduct my measurements, they have been and continue to be a constant source of inspiration of how dedication to patient care and respectful treatment of all people can be, and should be, in healthcare and beyond.

Contents

List of Tables.....	8
List of Figures.....	9
I. Introduction.....	11
Internal Kinetics of Radioactive Materials.....	11
Historic Releases of Radioactive Material into the Environment	13
Current radiobioassay methods	15
Proposed method of radiation detection and analysis	17
Monte Carlo Modeling	19
Review of past incidents.....	19
Basis for radionuclides considered in this dissertation	23
Current Guidance	25
Concept of Minimum Detectable Dose	27
II. Materials and Methods	31
Biokinetic Model for Urinary Excretion	31
Absorbed dose and dose equivalent.....	40
Gamma Camera Operation	40
Urine Specimen Collection and Analysis	44
Gamma Camera settings/protocol	45
Detector response to background radiation	45
Effect of sample volume on detector response	46
Gamma camera detector efficiency.	47
Cross talk between regions of interest.....	48
Monte Carlo Modeling	48
Minimum Detectable Dose.....	49
III. Results	50
Background Determination	50
Technitium-99m Validation of MCNP Model	52
MCNP derived efficiencies for radionuclides of interest.....	53
Crosstalk between adjacent regions of interest.....	58
Minimum Detectable Intake	63
Minimum detectable dose (MDD).....	65
IV. Discussion	67

Cobalt-60	69
Iodine-131	71
Cesium-137.....	72
Iridium-192.....	74
Volume Throughput	76
V. Limitations.....	77
VI. Conclusions.....	80
VII. References.....	81

List of Tables

Table 1: Historical Radiological Events

Table 2: Number of individuals impacted by the Chernobyl Accident

Table 3: Radionuclides of Interest

Table 4: Daily Urinary Excretion Fractions for the Radionuclides of Interest

Table 5: ROI Background Measurement

Table 6: Specifications for Tc-99m

Table 7: Tc-99m Activity Measurements in ROI

Table 8: MCNP Input Parameters for comparison to experimental results

Table 9: Detector efficiencies for photon energy ranges from 75 keV to 1400 keV

Table 10: MCNP-derived efficiencies for Radionuclides of Interest

Table 11: Calculated detector efficiency for radionuclides of interest with energy windows as a function of urine sample volume

Table 12: Background measurements at select gamma energy windows.

Table 13: MDI and calculation parameters for the radionuclides of interest

Table 14: MDD for cobalt-60 (t) days post incident

Table 15: MDD for iodine-131 (t) days post incident

Table 16: MDD for cesium-137 (t) days post incident

Table 17: MDD for iridium-192 (t) days post incident

List of Figures

Figure 1: Simplified biokinetic model for iodine

Figure 2: Logic diagram for converting Clinical Decision Guidelines to measurements of radionuclides in urine specimens

Figure 3: Simplified compartment model

Figure 4: General diagram for Biokinetics of radionuclides

Figure 5: Biokinetic Model for Cobalt-60

Figure 6: Biokinetic Model for Iodine-131

Figure 7: Biokinetic Model for Cesium-137

Figure 8: Biokinetic Model for Iridium-192

Figure 9: Reported NaI Detector Efficiencies for various photon energies and detector thicknesses

Figure 10 – Cross sectional view of a typical gamma camera detector

Figure 11 – Image of the General Electric Hawkeye V3 Gamma Camera

Figure 12 – Image of a urine specimen container placed on a General Electric Hawkeye V3 Gamma Camera detector

Figure 13: Detector response as a function of liquid column height

Figure 14: ROI array for background determination

Figure 15: Gamma Energy versus Detection Efficiency for the 3/8-inch and one-inch NaI crystal

Figure 16: Detection Efficiency vs Sample Size for 1 cm NaI Crystal

Figure 17: Detection Efficiency vs Sample Size for 2.54 cm NaI Crystal

Figure 18: Detector active surface area with ROI

Figure 19: Tc-99m Percent Count in ROI B from Sample in ROI A for Sample volume of 30, 60 and 90 ml

Figure 20: Tc-99m Percent Count in ROI B from Sample in ROI A for volume of 30, 60 and 90 ml

Figure 21: Cs-137 Percent Count in ROI B from Sample in ROI A for volume of 30, 60 and 90 ml

Figure 22: Cobalt-60 Percent Count in ROI B from Sample in ROI A for volume of 30, 60 and 90 ml

Figure 23: Cobalt-60 Crosstalk (%) for Separation Distances of ROI's from 0 - 19.5 cm

Figure 24: Iodine-131 Crosstalk for Separation Distances of ROI's for Separation from 0 - 19.5 cm

Figure 25: Cesium-137/Barium-137m Crosstalk (%) for Separation Distances of ROI's from 0 - 19.5 cm

Figure 26: Technitium-99m Crosstalk for Separation Distances of ROI's from 0 - 19.5 cm

Figure 27: Iridium-192 Crosstalk (%) for Separation Distances of ROI's from 0 - 19.5 cm

Figure 28: Background photon energy distribution for the GE Hawkeye V3, 3/8-inch NaI crystal

Figure 29: MDD for Cobalt-60 (Type F, S, M) days post incident

Figure 30: MDD for Iodine-131 (Type F, S, M) days post incident

Figure 31: MDD for Cesium-137 (Type F, S, M) days post incident

Figure 32: MDD for Iridium-192 (Type F, S, M) days post incident

I. Introduction

There have been several large-scale releases of radioactive material in the last forty years that have led to members of the public ingesting or inhaling radioactive materials. (Coeytaux, et al., 2015) This intake of radioactive materials can cause significant radiation contaminations which, concurrently, can increase the incidence of cancer in the contaminated populations. (ICRP, 2007) Unlike external exposures, which can be quickly stopped by moving out of the radiation field or cleaning contaminated surfaces, radioactive materials taken into the body only are removed through radioactive decay and biological elimination; yet the rate of biological elimination can be increased through timely medical intervention. Identifying which individuals have received an intake of radioactive material and which must receive medical intervention must occur soon after the contamination to limit the resulting radiation dose to that person. Yet, while techniques exist to monitor potential intakes by an individual, we presently lack the analytical capacity to quickly and accurately assess radioactive material intakes in a large group of people.

[Internal Kinetics of Radioactive Materials](#)

Radioactive materials from radiological events may be inhaled, ingested, absorbed, or injected into humans. The disposition of the radioactive material in a human body is a function of the chemical form and composition, size, and route of entry. (Bevelacqua, 2005) Once radioactive material is taken internally within a human body, the material will be removed from the body through radiological decay and biological elimination pathways such as through excretion in sweat, urine or feces. (ICRP, 2015)

As an example, iodine-131 is a common nuclear fission product that was released during the Chernobyl and Fukushima Daiichi nuclear accidents. (UNSCEAR, 2013) It also is widely used as a therapeutic agent for the treatment of thyroid diseases such as thyroid cancer and hyperthyroidism. Elemental Iodine is highly volatile and, when released into the environment, becomes adsorbed onto dust particulates in the air where it can be inhaled or ingested. Once inhaled, iodine is absorbed into blood as inorganic iodide. Iodine in the blood is either absorbed by the thyroid or cleared through the renal system as presented in the biokinetic model of Figure 1. Once absorbed by the thyroid, the Iodine is stored and, when needed, converted into a hormone, either thyroxine or triiodothyronine, which are secreted through the body to regulate metabolic processes critical for growth and development. (ICRP, 2017) More than 90% an intake of elemental iodine is eventually released by renal clearance (urine) 48 -72 hours post intake. Little of this intake is removed by fecal clearance or through sweat.

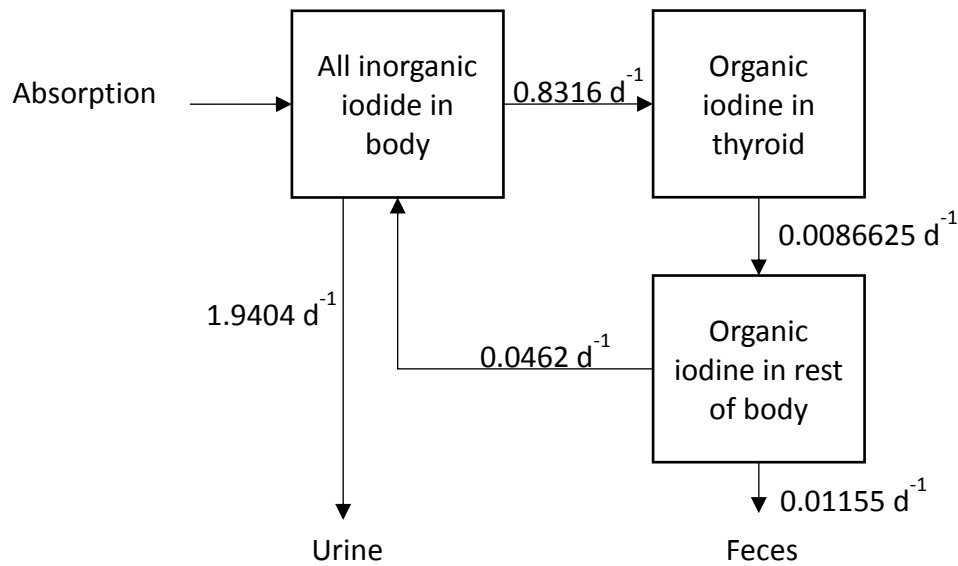


Figure 1: Simplified biokinetic model for iodine (ICRP 137, 2017)

Because of this, urine samples obtained after an accident can be used to estimate the amount of radio-iodine that was initially inhaled or ingested. Such samples typically must be collected within one week post intake since samples collected beyond this time contain mostly recycled inorganic-iodine, which is a small amount as compared to the amount excreted via urine in the first few days. Determining intakes from urine sample measurements collected beyond one week therefore is more difficult due to the lower concentrations of iodine-131 present in the urine sample.

[Historic Releases of Radioactive Material into the Environment](#)

Radioactive materials can be introduced into our environment either accidentally, such as the release of radioactive materials from the earthquake and tsunami-ravaged Fukushima Daiichi nuclear power plants in Japan, or intentionally, such as the assassination of Vladimir Litvinenko in England from polonium-210 poisoning in a public restaurant (Bailey, Etherington, Fraser, & Wilkins, 2010) and the release of cesium-137 in the Goiania incident. (Coeytaux, et al., 2015) Such incidents caused large numbers of the surrounding population to become concerned that they were “contaminated” by radiation or radioactive material. While experience has shown that the actual number of contaminated individuals is small, the number of *potentially* contaminated individuals is large. (EPA, 2017) We will refer to individuals with an unknown internal contamination status as being “potentially contaminated,” while individuals confirmed to have received an intake of radioactive materials through measurement as being “contaminated.” Individuals confirmed through measurement as not having received an intake are referred to as “non-contaminated.”

In past events, we have learned that efforts to identify and separate the affected from the non-affected population is time-consuming and difficult (EPA, 2017) with the limiting factors being the lack of analytical equipment to perform the measurements, lack of trained personnel in using and interpreting the results from the measurements, and the inability to relocate the needed analytical equipment in a timely manner. (IAEA, 1988) (Ansari & Caspary, 2015) It would be advantageous, therefore, to develop a precise and accurate technique for assessing potential radiation intakes and contaminations to ensure that resources, appropriate medical care and timely countermeasures can be focused where needed.

Currently, potentially contaminated individuals are tested for radiological intakes using specialized equipment such as a whole-body counter, hand-held radiation detecting equipment, or collection of excreta sent off-site for analysis. This is a major limitation of current practices of testing large numbers of potentially contaminated people; for example, it took four months to initiate the first measurements to identify intakes of radioactive material to the population surrounding the Daiichi Nuclear Power Plant. (Nomura, et al., 2015) The reason for the delay was that the measurements required a special instrument (whole body counter) to be brought to a nearby site, and that each person had to be measured individually. In addition, the elevated background radiation levels limited the devices accuracy (sensitivity) which resulted in the decision to move the device to a new location. Ultimately, this 4-month delay prevented our ability to accurately and precisely detect iodine-131 intakes because of iodine's three month biological and radiological removal rate from the body. (Nomura, et al., 2015)

Current radiobioassay methods

Radioactive material in the body can be measured through a variety of methods. (Bevelacqua, 2005) For example, one can directly measure radioactive material *in vivo* by using instruments that detect photon radiations emitted from the radioactive material. Alternatively, one could indirectly measure an intake of radioactive material, *in vitro*, by collecting and analyzing biological samples taken from the body, such as hair, tissue, blood, urine or feces. The quantity of the radioisotope in these samples are directly related to the amount of radioactive material that entered the body.

The type of radiobioassay that should be performed on a person potentially contaminated by radioactive material depends on specific factors including:

- The time of intake,
- The mode of intake (e.g., inhalation, ingestion, wound, etc.),
- If the intake is from a single radionuclide or multiple radionuclides,
- The chemical and physical form, such as the particle size or solubility, of the radionuclide,
- The rate of decay of the radionuclide, and
- The metabolic characteristics and behavior of the radionuclide in the body.

Currently, the most common method to radiobioassay a person potentially contaminated by radioactive material involves the *in vivo* monitoring of that person; this individual therefore must be present during the monitoring period, and only one person can be monitored at a time for each radiation detector. Only photon-emitting radioactive material can be measured

using this method because the other forms of radiation, i.e., beta or alpha radiation, is not capable of penetrating the human tissue and be detected by a radiation measuring instrument. Persons analyzed using this method are placed in a chair and one or more gamma sensitive radiation detectors are placed in close proximity to an area of the body, such as the upper torso, to measure the presence of radioactive material in the lungs. Another common in vivo radiobioassay is the use of a NaI detector to measure the presence of the gamma-emitting radionuclide iodine-131 in the thyroid of a person. A small NaI crystal, such as a 2-inch x 2-inch crystal is placed close to a person's thyroid gland and detects the gamma emissions from the presence of any iodine-131. The typical amount of time to perform a measurement varies as a function of the energy of the gamma ray, and the frequency of how often the gamma ray is emitted by the radioactive material which will be used to adjust counting times to reach the desired level of sensitivity.

One study reported on the application of the gamma camera to in vivo radiobioassay in individuals. (Anigstein, Olsher, & Loomis, 2010) A gamma camera has two large area radiation detectors (a.k.a. gamma camera heads). A more detailed discussion on the design of the gamma camera is discussed in a later section. The person is placed between the two gamma camera heads and used to detect the presence of gamma-emitting radionuclides. There are several limitations with this method. Detector efficiency determinations required sophisticated modeling techniques. A significant limitation is the detection efficiency is predicated on knowing the geometry of various body habitus of individuals and having them properly positioned between the two gamma camera heads so appropriate correction factors can be applied to the results. In addition, interpretation of the results is complicated and

requires specialized knowledge; estimating the quantity of radioactive material in a specific organ is needed to estimate intake and the gamma camera would require several (tens of minutes) to achieve the desired level of sensitivity. This method greatly limits the number of people that can be assessed because of measurement preparation, and a lack of professionals who can interpret the data.

In vitro bioassay monitoring is performed through urine and fecal testing. Here, a potentially contaminated person submits a sample which is analyzed with a radiation detector to quantify the presence of radioactivity in terms of the source activity (rate of radiological decay) and to identify the radioactive isotope. Once quantified, this information can be used to estimate the total intake of radioactive material and the resulting radiation contamination the person will receive from that intake. These estimations, both, *in vivo* and *in vitro* monitoring, are evaluated according to various biokinetic models which predict the average biological transport of the isotope through the body. (ICRP, 2015)

In vitro radiobioassay has the significant advantage that samples can be collected remotely and delivered to a hospital nuclear medicine department for analysis. Additionally, analysis methods are simpler to implement, the results are simpler to interpret, and a large number of samples can be analyzed concurrently. *In vitro* radiobioassay does require staff trained in use of the gamma camera, a CLIA certified laboratory, and appropriate equipment.

[Proposed method of radiation detection and analysis](#)

The goal of this dissertation is to present a method for the use a nuclear medicine gamma camera to conduct high volume throughput quantitative analyses to accurately and precisely evaluate radionuclide intakes.

Gamma cameras are used to detect gamma rays and x-rays, hence, radioactive materials that primarily emit alpha or beta radiation were eliminated from further evaluation. This limitation did not have a large impact on the utility of our technique because almost all radioactive isotopes emit gamma rays and x-rays. Although, some radioactive isotopes emit gamma rays so infrequently that use of the developed technique is not practical. These radioactive isotopes were similarly excluded.

A standard nuclear medicine gamma camera (General Electric Hawkeye V3) was used to measure the detection efficiency for technetium-99m (Tc-99m), which is a frequently used radionuclide in the nuclear medicine department. The gamma camera was then modeled using MCNP v6.0 (LANL, 2017) to calculate detector efficiency for Tc-99m to compare the measured versus modeled results. Verification and acceptance of the gamma camera model allowed the calculation of detector efficiencies for radionuclides not available for empirical analysis. Detector efficiencies for the radionuclides of interest were used to develop the lower limit of detection and minimum committed effective dose for comparison to accepted regulatory guidelines.

The bioassay method in this dissertation employs the use of a standard gamma camera to concurrently analyze a group of urine specimens. A gamma camera is a device used in nuclear medicine departments in hospitals for the diagnosis of diseases and medical conditions. Radioactive materials chemically attached to pharmaceuticals are intentionally administered to the patient for the purpose of monitoring its physiological disposition via images produced by the gamma camera. The gamma camera employs a large area radiation detector sensitive to x- and gamma rays that, once detected, create images visible on a computer display. The

use of a gamma camera to analyze bioassay samples is demonstrated with emphasis on the accuracy, sensitivity, and capacity to meet the time-critical needs for clinical decision-making post a radiological event.

[Monte Carlo Modeling](#)

Monte Carlo N-Particle (MCNP6.2) transport code (LANL, 2017) was developed by Los Alamos National Laboratory in 1957. It has been continually updated and improved to the present. It is used primarily to simulate nuclear processes and is applied to a wide variety of areas where radiation interactions must be calculated. The software allows the generation of three-dimensional models with radiation-related characteristics assigned to all molecules in the design. A calculation involves the tracking of a single radiation particle, e.g., photons, electrons, neutrons, from the initial point of interaction with a molecule in the model to the end of its path, or when it exits the area of interest. Each interaction results in the deposition of energy in the media per unit mass of that material (i.e., absorbed dose). The software tracks the complete history of all interactions, and hence dose deposited, for each radiation particle included in the simulation. For this dissertation, MCNP v6.0 was used to model a generic NaI detector, a urine specimen container, and urine media in the geometry expected to occur for a gamma counter. Photon histories were used to quantify radiation detection events in the NaI crystal as a function of the number of photons emitted by the radionuclide of interest (i.e., detection efficiency).

[Review of past incidents](#)

Literature detailing actual radionuclide releases were evaluated to identify the radionuclides of concern for public dose. The list of radionuclides was reviewed for the type of radioactive

emissions and their detectability using a standard gamma camera. Table 1 summarizes the large-scale radiological incidents that have occurred over the past 40 years; this table includes the year the event occurred, the radionuclides released to the environment, the number of people potentially affected, the number of people verified as affected, and the time to perform initial intake measurements on members of the public.

Table 1: Historical Radiological Events

Event	Year	Type	Radionuclides released	# Potentially affected	# affected	Time to Initial Bioassay
Three Mile Island (Battist & Peterson Jr., 1979)	1979	Nuclear Power accident	⁸⁵ Kr, ¹³¹ I, ¹³³ Xe	2,000,000	2 million (est.)	None performed
Chernobyl (UNSCEAR 2008 Report: Vol. II)	1986	Nuclear Power accident	⁸⁵ Kr, ¹³¹ I, ⁹⁰ Sr, ⁶⁰ Co, ¹³⁷ Cs, ¹³³ Xe	Residents of northern hemisphere	500 million (est.)	1988
Goiania Brazil (IAEA, 1988)	1987	Irradiator accident	¹³⁷ Cs	112,000	249	Four months
Litvinenko (Harrison, et al., 2017)	2006	Intentional poisoning	²¹⁰ Po	990	137	1 month
Fukushima Daiichi (Samet & Chanson, 2015)	2011	Nuclear Power accident	⁸⁵ Kr, ¹³¹ I, ⁹⁰ Sr, ⁶⁰ Co, ¹³⁷ Cs, ¹³³ Xe	Residents of northern hemisphere	32 million (est.)	4 months

Three Mile Island (Ahearn, 1979) (Battist & Peterson Jr., 1979) The Three Mile Island Unit 2 reactor, near Middletown, Pa., partially melted down on March 28, 1979. Investigations revealed a combination of equipment malfunctions, design-related problems, and worker errors led to TMI-2's partial meltdown and very small off-site releases of radioactivity. This

was the most serious accident in U.S. commercial nuclear power plant operating history, although its small radioactive releases had no detectable health effects on plant workers or the public.

The primary releases from TMI included krypton-88, xenon-133, xenon-133m, xenon-135, xenon-135m and iodine-131. The number of people potentially impacted by TMI was estimated as 2 million people. The majority (>99%) of the radioactivity released to the environment during the event were noble gases which are inhaled and immediately exhaled from the body resulting in no measurable radiation intake. No internal assessments of radiological intakes were conducted for members of the public following this incident.

Chernobyl - On April 26, 1986, human error and plant design flaws led to the steam explosion and complete meltdown of the graphite-moderated nuclear reactor. Within a few weeks of the accident, 30 workers had entered the area without proper respiratory protection died from radiation contamination and radiation injuries occurred to several hundred other workers. Large areas of Russia, Belarus, and Ukraine were radioactively contaminated. Contamination of the population was primarily caused by releases of iodine-131 (internal contamination), cesium-134 and-137 (internal contamination and external exposure). (UNSCEAR, 2008) Other radionuclides of biological significance released included plutonium-239, 240 and 241, and americium-241 (due to ingrowth from the decay of plutonium-241).

The number of people potentially impacted by the event was not provided, but radioactivity was reported as being measured in all countries in the northern hemisphere. (UNSCEAR, 2008) Impacted individuals were reported as 98 million for Belarus, Ukraine and Russia collectively, and 500 million for inhabitants of distant countries. Assessment of intakes in the

general public was initially performed within one week for 30 individuals in the Czech Republic, but wide-scale measurements for the population were not performed until two years post event. Table 2 presents the number of individuals, average thyroid dose and average effective dose from the Chernobyl accident.

Table 2: Number of individuals impacted by the Chernobyl Accident

Population group	Size (thousands)	Average thyroid dose in 1986 (mGy)	Average effective dose in 1986 –2005 (mSv)
Recovery operation workers	530	Not available	117
Evacuees	115	490	31
Inhabitants of contaminated areas of Belarus, Russia and Ukraine	6,400	102	9
Inhabitants of Belarus, Russian Federation and Ukraine	98,000	16	1.3
Inhabitants of distant countries	500,000	1.3	0.3

* Adapted from UNSCEAR 2008 Report Volume II

Goiania (IAEA, 1988) – On September 13, 1987, a sealed source containing cesium-137 was removed from an abandoned teletherapy device and subsequently intentionally ruptured releasing its contents into the environment. The nature of the source contents was unknown to those who ruptured the source. The radiological nature of the accident was not discovered until September 29, 1987. In the ensuing two weeks, news of the accident spread to the population and more than 129,000 people converged on the local Olympic Stadium to be screened. A total of 249 people were identified to be contaminated with cesium-137. Of this group, 129 people also had ingested and/or inhaled radio-cesium. The lack of trained personnel and instrumentation were identified as significant barriers to an effective response.

Litvinenko (Harrison, et al., 2017) – On 1 November 2006, a former Russian spy, Alexander Litvinenko, became ill after meetings with a former colleague at a sushi bar and hotel in London England. Three days later he was admitted to a local hospital and subsequently suffered a heart attack and died in the hospital on 22 November 2006. The radioisotope (polonium-210) was not identified until 24 November 2006. A total of 990 people were potentially contaminated by the polonium-210. Of this group, 779 people were offered to have their urine analyzed and 738 agreed. Of the 738 urine samples collected and analyzed, 137 had positive results. The quantity of polonium-210 detected in the 137 persons was low and not life threatening.

Fukushima - (Samet & Chanson, 2015) On 11 March 2011, the Fukushima Daiichi Nuclear Power Plant incident, resulted in an acute intake of iodine-131 and cesium-137 in the initial stage of the incident and was the primary source of internal radiation contamination (Tsubokura et al. 2013). From March 26-30, 2011 limited in-vivo sampling was performed of 1,080 individuals for iodine-131. By July 2011 internal contamination screening was performed using a chair-type Whole Body Counter (WBC) (Anzai Medical Co. 2014). Between 11 July 2011 and 29 July 2011 a sodium iodide (NaI) detector (5-inch diameter 3-inch thickness) was mounted on the back of a chair, and from that location, was able to count gamma isotopes (Hayano et al. 2014). However, the chair-type WBC provided insufficient shielding against background gamma rays. It was replaced by a better-shielded standing-type WBC (FASTSCAN Model 2251, Canberra Inc., USA) on 26 September 2011.

[Basis for radionuclides considered in this dissertation](#)

Radioactive materials could be released into the environment from events such as a fire at a

nuclear power plant, nuclear fuel manufacturing facility, radioactive source manufacturing facility, or a radioactive material use laboratory. Intentional incidents include intentional damage to nuclear facilities described above, radiological dispersal devices involving small and highly localized sources, the dispersal of large amounts of radioactive materials over large areas, and finally nuclear weapons, whether resulting in a nuclear yield or not.

The geographic extent of radiological hazards following an incident will depend on the radioactive material involved, and the mechanism by which it was released to the environment, e.g., fire, explosion, etc., and the environmental conditions at the time of the incident. Once taken into the human body, the disposition and elimination of the radioactive material will depend on its physical and chemical properties.

During and immediately after a radiological incident there are many decisions that must be made in a short period of time by a range of governmental organizations. (EPA, 2017) (Ansari & Caspary, 2015) Decisions must be made by appropriate organizations in the interests of law enforcement, public health and safety, damage to infrastructure, psychosocial impacts, and environmental concerns.

Many of the decisions are based upon the availability of data, and the results of models used to estimate potential impacts. Human radiation contamination data immediately following an incident is difficult to obtain due to logistic demands for responding to the event, and the lack of radiological instrumentation sufficient to handle the capacity needs, and trained individuals to perform the measurements. Employing countermeasures to reduce radiological uptake to humans is possible only if accurate information can be received in a timely manner. (Nomura, et al., 2015)

Based on these events and consideration of possible future terrorist-related events, Table 3 presents the radionuclides selected for evaluation as isotopes of concern for this proposed technique:

Table 3: Radionuclides of Interest

Radionuclide	Half-life	Emission type
¹³¹ I	8.1 days	β, γ
¹³⁷ Cs/ ^{137m} Ba	30.1 years	β, γ
⁶⁰ Co	5.27 years	β, γ
¹⁹² Ir	73.8 days	β, γ

Radioactive isotopes, such as polonium-210, with negligible gamma yields (i.e., infrequent emissions) were excluded from the radionuclides of interest.

Current Guidance

The Centers for Disease Control (CDC), Radiation Studies Branch, addressed population monitoring after a radiological incident in a 2014 report (CDC, 2014) The CDC defines population monitoring as “a process that begins after a radiation incident is reported and continues until all potentially affected people have been monitored and evaluated for:

- Needed medical treatment
- The presence of radioactive contamination on the body or clothing
- The intake of radioactive materials into the body
- The removal of external or internal contamination
- The radiation dose received and the resulting health risk from the contamination long-term health effects”

The CDC guide is intended to advise emergency response personnel on the processes needed for monitoring potential intakes in a population contaminated by radioactive materials. Bioassay samples are identified as a powerful diagnostic tool for assessing internal contamination, and in the event of radiological dispersal, the urine sample is the most useful for dose estimation. Laboratory analysis capabilities are identified as a critical part of planning and should address:

- Analytical capability
- Sample prioritization and triage
- Turnaround time
- Sample throughput
- Sample volume
- Sample storage capacity
- Confidentiality assurance
- Protocols for reporting analytical result"

Analytical laboratories must also be capable of complying with Clinical Laboratory and Improvement Amendments (CLIA). CLIA certifies that a laboratory has the necessary equipment, personnel and procedures to accept human specimens for the purpose of performing specific laboratory procedures.

The National Council on Radiation Protection and Measurements published Management of Persons Accidentally Contaminated with Radionuclides: Handbook, Report No. 161. (NCRP, 2013) The guidelines are expressed as a dose (excluding isotopes of iodine) as:

- 0.25 Sv (50-year effective dose) whole body
- 0.25 Gy-Eq (30 day RBE-weighted absorbed dose) to the bone marrow
- 1 Gy-Eq (30-day RBE-weighted absorbed dose) to the lung

Iodine is excluded because it concentrates in the thyroid gland and the highest contamination for an intake is to the thyroid rather than the whole body.

The values are for adults. For children and pregnant women, the screening value is reduced to 20% of the CDG. The screening value for isotopes of iodine is age dependent. The limiting dose for which countermeasures are recommended is 0.05 Gy (i.e., for children up to 18 and pregnant or lactating women). These values are consistent with guidance issued by the International Commission on Radiological Protection. Figure 2 shows the logic diagram for converting the Clinical Decision Guideline (CDG) to a quantity of a radionuclide that would be measured in urine at a time “t” post-incident.

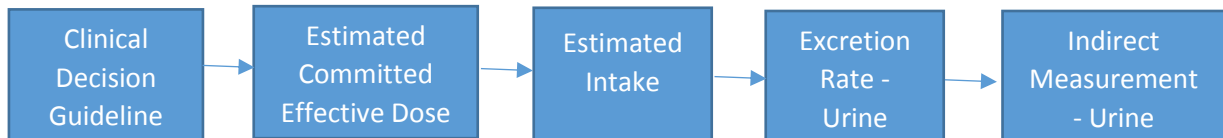


Figure 2: Logic diagram for converting Clinical Decision Guidelines to measurements of radionuclides in urine specimens

Concept of Minimum Detectable Dose

For this technique to be useful, it must have the precision to measure the radiation contamination detailed in NCRP 161. To that end, the minimum detectable dose (MDD) is a statistical characterization of the device’s radiation detection limits based on accepted *a priori* assigned confidence levels. (Currie, 1968) Because radiation is also present in our natural environment, background radiation will act as a confounding factor in any

measurement. Therefore, we must apply a statistical test to separate a true positive sample from one that is indistinguishable from background radiation. The test involves establishing a null hypothesis (H_0) and an alternative hypothesis (H_1). The null hypothesis is the general statement that no activity is present in the sample while the alternative hypothesis is the statement that activity is present in the sample. (Currie, 1968)

We will use a sample containing no radioactivity to serve as our control sample (blank). Our blank sample then is measured by the gamma camera's NaI detector to quantify the background radiation contribution to a sample. However, to determine our MDD we are only interested in accounting for those gamma rays that are of the same energy as for the radiation we are looking to detect. We accomplish this by placing a "window" around the energy peak of interest and we can count the number of detections from background radiation. The distribution of counts in this region can be characterized by a population mean (μ_B) and standard deviation (σ_B). If we place a sample on the detector and count the number of detections within that energy window we can express the mean count (C_B) and the standard deviation (s_B). The net count is obtained by subtracting the background counts from the sample counts. This will result in a zero-mean count frequency distribution that is approximately normally distributed (bell-shaped). The standard deviation of the distribution is obtained by propagating the individual standard deviations of the terms.

$$\sigma_0 = \sqrt{\sigma_B^2 + s_B^2} \quad (\text{Eq. 1})$$

This distribution is used to determine a critical level to decide when activity is present. The critical level, L_c , is the net count in a zero-mean count distribution that has a probability of being exceeded. The general practice is to set the probability (α) at 5% meaning that we

expect one out of every twenty blank samples analyzed on our system to produce a signal that exceeds our critical level, L_c , by random chance alone. To summarize, if a sample count is less than the critical level, we accept the null hypothesis and conclude that no activity is present in the sample. Alternatively, if the count is above the critical level, L_c , then the null hypothesis is rejected and we conclude activity is present in the sample. In the case of our blank sample, we expect that twenty measurements of this sample will have one measurement that will exceed L_c for an $\alpha = 5\%$. Therefore, we also expect that if we measure twenty blank samples, one of those samples will exceed L_c which would cause us to incorrectly conclude that activity is present in the sample when in fact there is none (i.e. a false positive). In this case, the critical level is calculated as:

$$L_c = k_\alpha \sigma_B \quad (\text{Eq. 2})$$

Where k_α is the value of the standard normal deviation for a normal distribution using a one-tailed level of $1 - \alpha$. The corresponding value of k_α is 1.645 for an $\alpha = 5\%$. Therefore, coupling Eq 1 and Eq. 2, the critical level for a sample containing no activity measured in the presence of background radiation (that is, the standard deviation of the sample and background would be equal so that $\sigma_B = s_B$) becomes:

$$L_c = 1.645 \sqrt{2s_B^2} = 2.33 s_B^2 \quad (\text{Eq. 3})$$

Based on our critical limit, we next can derive a detection limit, L_D , which is the number of counts that the detector can “detect” with a confidence level β . The detection limit typically is larger than L_c based on our decision criteria, β , to allow our detector to obtain a false negative (that is, radiation is present on our sample but creates a measurement that is lower

than L_d . L_d is typically chosen to produce a false negative at 5% confidence and will almost always will correctly determine that activity is present. However, similar to L_c , the counts are distributed normally and it is common to select a probability of 5% meaning that we will accept the probability of stating that no activity is present when it is present. The equation for L_D is:

$$L_D = L_C + k_\beta \sigma_D \quad (\text{Eq. 4})$$

Where k_β is the value of the standard normal deviate for the normal distribution using a one-tailed probability. Replacing like variables we see L_D is:

$$L_D = C_S + (C_B - \mu_B) \quad (\text{Eq. 5})$$

The standard deviation is obtained by propagating the errors in the gross count.

$$\sigma_D = \sqrt{(C_S + \sigma_0^2)} = \sqrt{L_D + \sigma_0^2} \quad (\text{Eq. 6})$$

Solving for L_D yields:

$$L_D = 2.71 + 4.65 s_B \quad (\text{Eq. 7})$$

This L_D describes the net count having a 95% probability of being detected when a sample contains activity at L_D , and a 5% probability of incorrectly concluding that activity is present when it is not. (Currie, 1968)

The area of the detector that is used to measure the sample and background is limited to a smaller area of the detector called the Region of Interest (ROI). Converting this value of L_D to the dose that corresponds to this detection level takes into account a correction for the number of gamma rays emitted by the radionuclide at energy E (Y) and the efficiency of the

detector to count gamma rays of the energy E. Urine samples are expressed in units of activity per unit volume of the urine being measured. This value is then normalized to the reference man daily excretion of urine (1400 ml/day). (ICRP, 2015) These factors result in the Minimum Detectable Intake (MDI):

$$MDI (Bq) = \left(\frac{2.71 + 4.65\sqrt{B_{ROI}}}{Y_n \left(\frac{Y}{d}\right) E_n \left(\frac{c}{\bar{Y}}\right) \left(\frac{V_s(ml)}{1400ml}\right)} \right) \text{ (Eq. 8)}$$

Where B_{ROI} is the background counts in the region of interest, Y_n is the photon yield of energy E_i , and E_n is the efficiency of the detector for the n^{th} radionuclide of interest, and V_s is the volume of urine in the specimen container normalized to reference man daily urinary excretion. The minimum detectable dose (MDD) is then calculated by multiplying the MDI by the urinary excretion fraction expressed as dose per unit intake for a specific radionuclide or:

$$MDD (Sv) = MDI(Bq) \times UEF \left(\frac{Sv}{Bq} \right) \text{ (Eq. 9)}$$

II. Materials and Methods

We are investigating using a gamma-camera to detect radioactive materials in the urine bioassay of a potentially contaminated person. The intake, and therefore the expected radiation absorbed dose delivered to the person, can be estimated using a Biokinetic Model that simulates the transport of the radioisotope through the body and ultimately deposited into urine.

[Biokinetic Model for Urinary Excretion](#)

The biokinetic model to estimate the number of radiological decays that occur in the human body and transfer of the radioactive elements from one organ or “compartment” to another

is mathematically derived using general kinematics which assumes that the rate of transport from one compartment to the next and that the rate of radiological decay remains constant. This results in a series of first order differential equations that can be solved to determine the number of radioactive atoms in a specific compartment at a time “t” post intake. For example, a simplified three compartment model is described in Figure 3:



Figure 3: Simplified compartment model

where, N_i is the removal of radionuclide in the i^{th} compartment to the next, and lambda (λ) is the removal rate for that compartment. The removal rate is a combination of the decay constant and biological removal constant from the compartment (i).

The removal rate is constant for each compartment and can be shown as thus,

$$\text{Compartment 1: } \frac{dN_1(t)}{dt} = -\lambda_1 N_1(t) \quad (\text{Eq. 10})$$

$$\text{Compartment 2: } \frac{dN_2(t)}{dt} = +\lambda_1 N_1(t) - \lambda_2 N_2(t) \quad (\text{Eq. 12})$$

$$\text{Compartment 3: } \frac{dN_3(t)}{dt} = +\lambda_2 N_2(t) - \lambda_3 N_3(t) \quad (\text{Eq. 13})$$

Rearranging the terms:

$$\frac{dN_1(t)}{dt} + \lambda_1 N_1(t) = 0 \quad (\text{i}) \quad (\text{Eq. 14})$$

$$\frac{dN_2(t)}{dt} + \lambda_2 N_2(t) = \lambda_1 N_1(t) \quad (\text{ii}) \quad (\text{Eq. 15})$$

$$\frac{dN_3(t)}{dt} + \lambda_3 N_3(t) = \lambda_2 N_2(t) \quad (\text{iii}) \quad (\text{Eq. 16})$$

Using Laplace transforms to solve the three equations yields:

$$N_1(t) = N_1(0) e^{-\lambda_1 t} \quad (\text{Eq. 17})$$

$$N_2(t) = N_1(0) \lambda_1 \left[\frac{e^{-\lambda_1 t}}{(\lambda_2 - \lambda_1)} + \frac{e^{-\lambda_2 t}}{(\lambda_1 - \lambda_2)} \right] \quad (\text{Eq. 18})$$

$$N_3(t) = N_1(0) \lambda_1 \lambda_2 \left[\frac{e^{-\lambda_1 t}}{(\lambda_3 - \lambda_1)(\lambda_2 - \lambda_1)} + \frac{e^{-\lambda_2 t}}{(\lambda_3 - \lambda_2)(\lambda_1 - \lambda_2)} + \frac{e^{-\lambda_3 t}}{(\lambda_1 - \lambda_3)(\lambda_2 - \lambda_3)} \right] \quad (\text{Eq. 19})$$

The human body is more complicated in that it is generally represented with nine interrelated compartments as shown in Figure 4 below. The compartments that are impacted depend on the radionuclide chemical and physical form. For this dissertation, the biokinetic models used were those presented in ICRP 134 and 137. (ICRP, 2016) (ICRP, 2017)

Biokinetics of each radionuclide of interest in the human body is described by two sets of differential equations. The first set describes the number of atoms in the compartments during the intake of a radionuclide during an incident. The second set describes the processes after the termination of the intake.

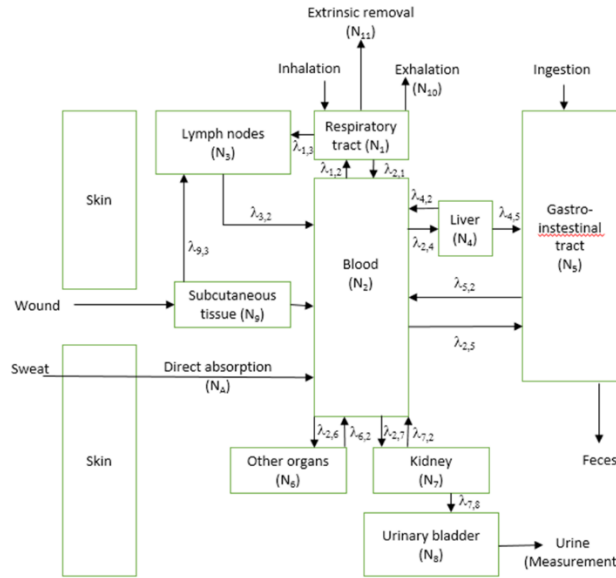


Figure 4: General diagram for Biokinetics of radionuclides

(Adapted from (ICRP, 2017))

The total number of atoms during an intake U is assumed to be constant for the individual and is given as:

$$U = \frac{A_0}{\lambda_s} \quad (\text{Eq. 20})$$

Where A_0 is the intake of activity, and λ_s is the decay constant for the radionuclide. The ratio

$$R = \frac{U}{T} \quad (\text{Eq. 21})$$

Where T is the duration of intake and yields the number of intake atoms per unit time. The duration of intake is dependent on the nature of the incident, the time to discovery of a release, and the time to remove the individual from the radiological environment. In this dissertation, it is assumed that the individual is removed from the radiological environment

and that intake via inhalation, ingestion, wounds and dermal absorption, and removal via exhalation and extrinsic mechanisms has been terminated (R=0).

Therefore, the differential equations describing the time rate of change in the number of atoms in each of the nine compartments post incident are as follows:

$$\frac{dN_1}{dt} = -\lambda N_1 - \lambda_{1,2}N_1 + \lambda_{2,1}N_2 \quad (\text{Eq. 22})$$

$$\begin{aligned} \frac{dN_2}{dt} = & -\lambda N_2 - \lambda_{2,1}N_2 - \lambda_{2,4}N_2 - \lambda_{2,5}N_2 - \lambda_{2,6}N_2 - \lambda_{2,7}N_2 + \lambda_{1,2}N_1 + \lambda_{3,2}N_3 + \\ & \lambda_{4,2}N_4 + \lambda_{5,2}N_5 + \lambda_{6,2}N_6 + \lambda_{7,2}N_7 \end{aligned} \quad (\text{Eq. 23})$$

$$\frac{dN_3}{dt} = -\lambda N_3 - \lambda_{3,2}N_3 + \lambda_{1,3}N_1 \quad (\text{Eq. 24})$$

$$\frac{dN_4}{dt} = -\lambda N_4 - \lambda_{4,5}N_1 - \lambda_{4,2}N_4 + \lambda_{2,4}N_2 \quad (\text{Eq. 25})$$

$$\frac{dN_5}{dt} = -\lambda N_5 - \lambda_{5,2}N_5 + \lambda_{4,5}N_4 + \lambda_{2,5}N_2 \quad (\text{Eq. 26})$$

$$\frac{dN_6}{dt} = -\lambda N_6 - \lambda_{6,2}N_6 + \lambda_{2,6}N_2 \quad (\text{Eq. 27})$$

$$\frac{dN_7}{dt} = -\lambda N_7 - \lambda_{7,2}N_7 - \lambda_{7,8}N_7 + \lambda_{2,7}N_2 \quad (\text{Eq. 28})$$

$$\frac{dN_8}{dt} = -\lambda N_8 + \lambda_{7,8}N_7 \quad (\text{Eq. 29})$$

$$\frac{dN_{9,10,11}}{dt} = 0 \quad (\text{Eq. 30})$$

Here, λ is the effective removal constant for the radionuclide (i.e., $\lambda_R + \lambda_B$), and N_i is the number of atoms in the N^{th} compartment. And $\lambda_{1,2}$, $\lambda_{1,3}$, $\lambda_{2,1}$, $\lambda_{1,2}$, $\lambda_{2,4}$, $\lambda_{2,5}$, etc. are transfer rates from one compartment to another. For example, $\lambda_{1,2}$ is the transfer rate from

compartment 1 to compartment 2. The value is negative (-) with respect to N_1 but positive with respect to N_2 .

The differential equations presented above are solved and the solution rearranged to calculate the urinary excretion at time (t) post termination of the intake.

The biokinetics for the systemic models for cobalt-60, iodine-131, cesium-137 and iridium-192 are presented in Figures 5 through 8, respectively. (ICRP, 2016) (ICRP, 2017)

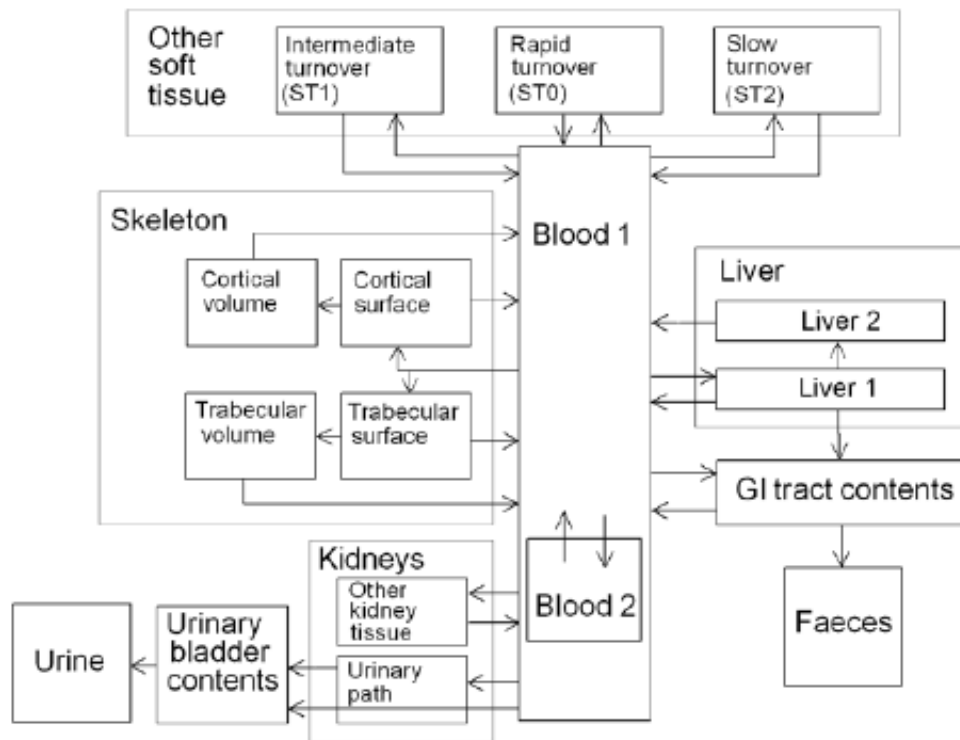


Figure 5: Biokinetic Model for Cobalt-60 (ICRP 134, 2016)

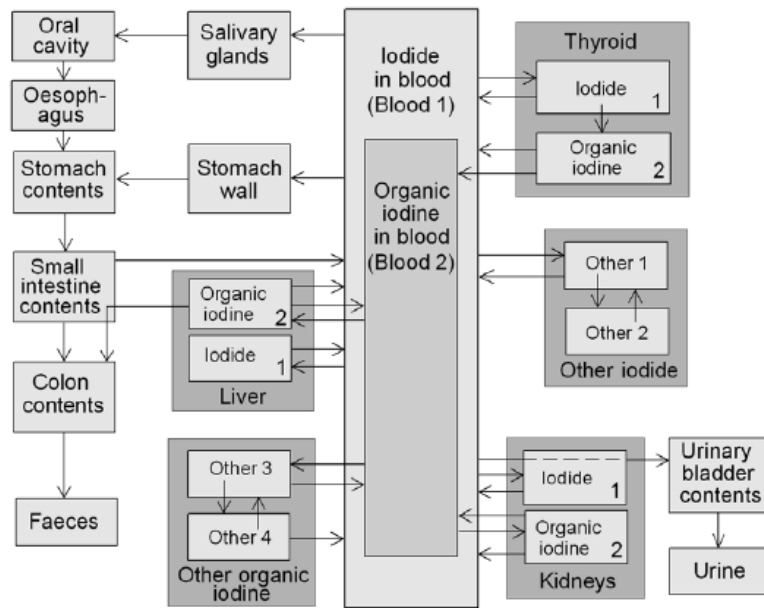


Figure 6: Biokinetic Model for Iodine-131 (ICRP 137, 2017)

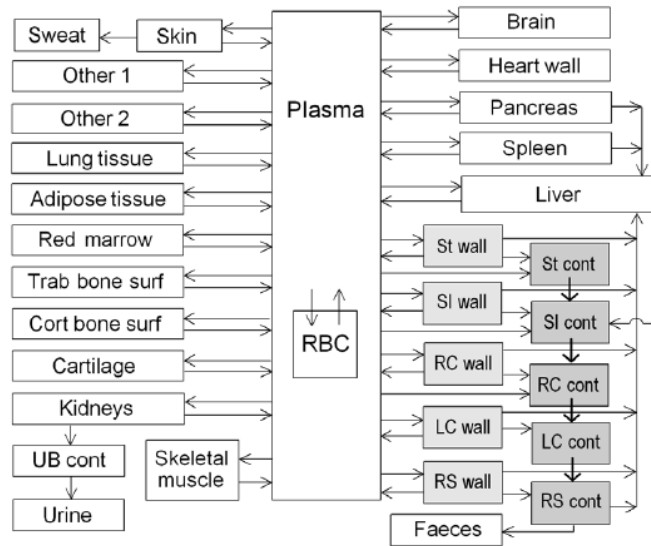


Figure 7: Biokinetic Model for Cesium-137 (ICRP 137, 2017)

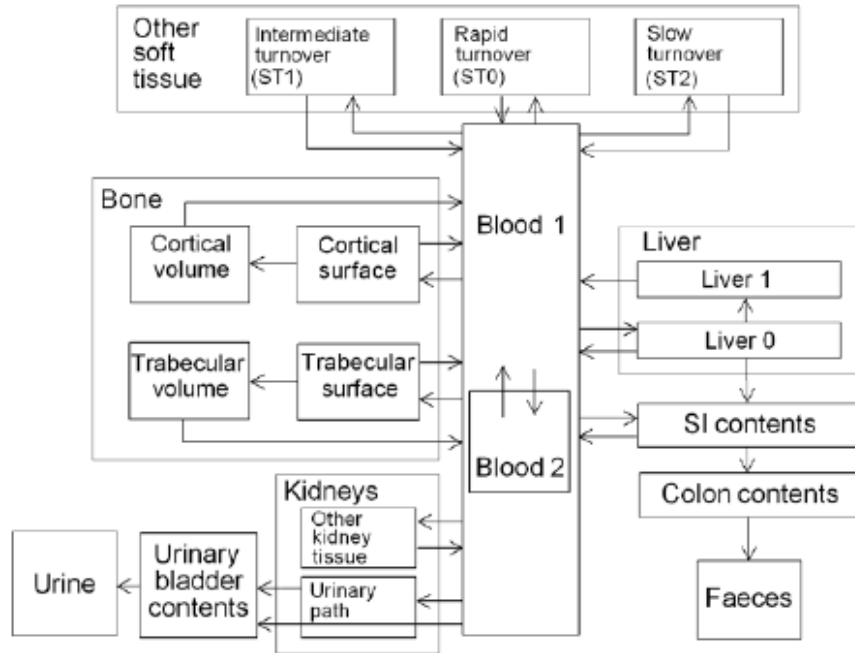


Figure 8: Biokinetic Model for Iridium-192 (ICRP 137, 2017)

The input parameters used to calculate intake and excretion were empirically determined through human and animal studies as presented in ICRP 130, 134 and 137. The resulting daily urinary excretion fractions as a percent of intake are presented in Table 4.

Table 4: Daily Urinary Excretion Fractions for the Radionuclides of Interest

Days	Co-60 (Sv/Bq) Fraction in daily urine			I-131 (Sv/Bq) Fraction in daily urine		
	Type F	Type M	Type S	Type F	Type M	Type S
1	1.30E-07	9.30E-07	9.30E-05	3.20E-08	4.30E-08	2.00E-07
2	3.10E-07	2.20E-06	2.20E-04	1.60E-07	1.30E-07	5.40E-07
3	5.50E-07	3.80E-06	3.90E-04	1.20E-06	9.00E-07	3.80E-06
4	8.10E-07	5.30E-06	5.50E-04	9.50E-06	4.80E-06	2.20E-05
5	1.10E-06	6.90E-06	7.30E-04	4.00E-05	1.10E-05	5.50E-05
6	1.40E-06	8.50E-06	9.20E-04	5.80E-05	1.40E-05	7.50E-05
7	1.70E-06	1.00E-05	1.10E-03	5.70E-05	1.60E-05	8.70E-05
8	2.10E-06	1.20E-05	1.30E-03	5.50E-05	1.80E-05	9.70E-05
9	2.60E-06	1.40E-05	1.60E-03	5.40E-05	2.00E-05	1.10E-04
10	3.00E-06	1.50E-05	1.80E-03	5.50E-05	2.20E-05	1.20E-04

15	5.50E-06	2.20E-05	2.80E-03	6.60E-05	3.40E-05	1.90E-04
30	1.50E-05	3.60E-05	5.10E-03	2.00E-04	1.20E-04	6.70E-04
45	3.00E-05	4.60E-05	6.60E-03	7.70E-04	4.80E-04	2.50E-03
60	4.80E-05	5.30E-05	7.50E-03	3.00E-03	1.90E-03	9.70E-03
90	7.90E-05	6.60E-05	8.50E-03	4.80E-02	3.00E-02	1.40E-01
180	1.80E-04	1.20E-04	1.10E-02	N/A	N/A	N/A
365	4.60E-04	3.50E-04	1.50E-02	N/A	N/A	N/A
Days	Cs-137 (Sv/Bq)			Ir-192 (Sv/Bq)		
	Fraction in daily urine			Fraction in daily urine		
	Type F	Type M	Type S	Type F	Type M	Type S
1	3.40E-07	1.20E-06	6.00E-05	6.00E-08	8.00E-07	2.30E-05
2	7.20E-07	1.90E-06	9.40E-05	3.10E-07	3.40E-06	9.90E-05
3	1.10E-06	3.10E-06	1.50E-04	4.90E-07	5.50E-06	1.70E-04
4	1.50E-06	4.20E-06	2.10E-04	6.40E-07	7.00E-06	2.10E-04
5	1.70E-06	5.00E-06	2.50E-04	7.90E-07	8.20E-06	2.60E-04
6	1.90E-06	5.60E-06	2.80E-04	9.40E-07	9.40E-06	3.00E-04
7	2.10E-06	6.10E-06	3.00E-04	1.10E-06	1.10E-05	3.40E-04
8	2.30E-06	6.50E-06	3.20E-04	1.20E-06	1.10E-05	3.80E-04
9	2.40E-06	6.80E-06	3.40E-04	1.40E-06	1.20E-05	4.10E-04
10	2.40E-06	7.00E-06	3.50E-04	1.50E-06	1.30E-05	4.50E-04
15	2.70E-06	7.70E-06	3.90E-04	2.20E-06	1.70E-05	6.00E-04
30	3.10E-06	8.70E-06	4.40E-04	4.90E-06	2.70E-05	1.00E-03
45	3.50E-06	9.70E-06	5.00E-04	8.00E-06	3.50E-05	1.40E-03
60	4.00E-06	1.10E-05	5.50E-04	1.10E-05	4.40E-05	1.70E-03
90	5.10E-06	1.30E-05	6.80E-04	1.90E-05	6.60E-05	2.40E-03
180	1.10E-05	2.40E-05	1.20E-03	6.90E-05	2.10E-04	6.10E-03
365	4.90E-05	8.70E-05	3.50E-03	7.50E-04	2.20E-03	4.10E-02

The daily urinary excretion fraction for each radionuclide is derived from empirical data taken from actual intakes of the radionuclide by humans during an unintentional contamination, or by humans and animals for surrogates used in controlled laboratory settings. The pathways for the radionuclides assessed are via inhalation and ingestion based on the Human Respiratory Tract Model. This model allows for three “Types” of absorption using experimental data, Type F (fast), Type M (Moderate) and Type S (Slow). Type F assumes that the amount absorbed into blood by 30 days after an intake is greater than a similar material

with a constant rate of absorption into blood with a half-time of 10 days. Type S is assumed if a similar element were absorbed into blood with a constant rate of absorption of 0.001 per day. If insufficient data exists, the ICRP recommends using a Type M for most elements as a default. (ICRP, 2015)

[Absorbed dose and dose equivalent](#)

The presence of radioactive material in an organ results in its emitted radiations being absorbed by the tissue and cells of the organ. Some radiation can also escape the organ and interact and be absorbed in adjacent organs. Energy absorbed by cells cause damage to the cellular components including the DNA. Such damage is usually repaired by cellular mechanisms, but can also lead to mutations that cause cancer. The energy absorbed by the tissues is described as “absorbed dose” and is expressed in units of Joules per kilogram. Outcomes to persons receiving absorbed doses to an organ have been extensively studied. Quantitative risk of cancer development and other detrimental effects from absorbed doses have been published (ICRP, 2007) and are expressed in terms of a dose equivalent. The dose equivalent is therefore a measure of the biological damage to living tissues from radiation contamination. It is expressed in units of Sieverts. (Koenig, et al., 2005)

[Gamma Camera Operation](#)

The gamma camera is used to image the distribution of a radioactive pharmaceutical in a patient for diagnostic purposes. A sodium-iodide or solid-state detector is used to detect the gamma or x-ray emissions from the radioactive component of the radiopharmaceutical in the patient, and the detected emissions are processed by a computer and software to produce a two or three-dimensional image. A gamma camera may have one or two detectors that pass

over the patient while lying motionless on a table. The detectors are mounted on a gantry and rotate in a circle around the patient to produce the three dimensional, i.e., tomographic, image. (GE, 2012)

Typical sodium iodide crystals range from 6.4 to 12.7 mm in thickness for most commercially available systems. The crystal thickness is intended to optimize detection efficiency and intrinsic spatial resolution. The energies the gamma camera is used to detect in nuclear medicine applications range from 100 to 200 keV. Thicker crystals are used to improve the detection efficiency for higher energy gamma emitter such as the 511keV photons produced from Fluorine-18 used in positron emitting tomography. The 2π detection efficiency for photon energies from 100 to 200 keV for various thicknesses is presented in Figure 9 below.

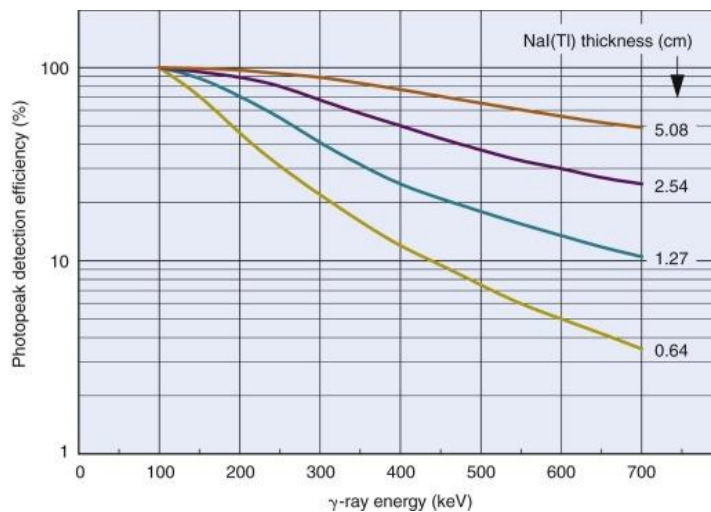


Figure 9: Reported NaI Detector Efficiencies for various photon energies and detector thicknesses (Adapted from Anger HO: Radioisotope cameras. (Hine, 1967)

Modern crystals are typically rectangular in shape with sizes up to 40 cm x 60 cm. Older style gamma cameras employed round crystals 25 to 50 cm in diameter. Below the crystal is an array of photomultiplier tubes coupled to the crystal by a layer of silicone-based adhesive. The tubes are arranged in a hexagonal fashion to optimize coverage of the detector area. The entire detector and PM tube assembly is light-tight and lead-lined to reduce background sources of signal. Typical PM tubes are about 5 cm in diameter, and a single crystal may be monitored by 15 to 60 tubes. There are various detector/PM tube designs that are intended to minimize signal distortion and loss. A schematic cross-section of a gamma camera assembly is presented in Figure 10 below.

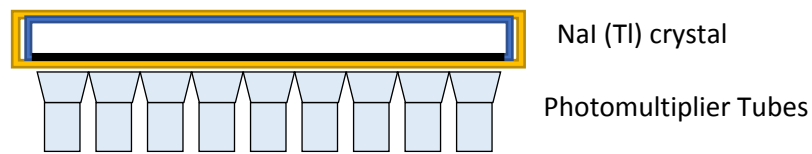


Figure 10 – Cross sectional view of a typical gamma camera detector

Current gamma cameras have an energy resolution of 9% to 10% and the detection efficiency is typically about 12% at 140 keV. However, the detector efficiency is a function of the detector thickness and energy of the photon.

The software used to analyze the signal and produce a two or three-dimensional image is unique to the manufacturer of the gamma camera. In general, an image is displayed on a computer monitor. For this study, two-dimensional images were produced, and the software used to draw a region of interest in the monitor's pixel array, and a summation of the detected photons within the region.

The gamma camera used for the measurements was a General Electric Hawkeye V3. (See Figure 11.) The Hawkeye consists of two heads each possessing a 3/8-inch thick NaI crystal backed by 59 photomultiplier tubes. The detectable energy range is reported by GE for this thickness crystal is 40 – 520 keV. (GE, 2012) There is a one-inch thick crystal model available as well with the detectable energy range extending to 900 keV. The gamma camera is used to analyze a plastic container containing simulated urine (See Figure 12). For the purposes of this dissertation, water was used as a surrogate for urine. Water was selected because there are no significant differences in radiation attenuation properties between urine and water. Detector intrinsic spatial resolution and detector efficiency is a function of the following variables - gamma energy, photon flux at the detector surface, and the height and areal extent of the liquid volume in the cylindrical specimen container. The experimental method to address each of the variables is discussed.



Figure 11 – Image of the General Electric Hawkeye V3 Gamma Camera (Courtesy of Lahey Medical Center, Burlington MA)

Urine Specimen Collection and Analysis

The advantage of this method is that hospitals commonly use gamma cameras and frequently use Urine specimen containers. Containers of urine specimens are placed on a gamma camera “head” housing the detector. Samples are counted for a specific time interval. The detected “counts” of radioactivity are converted into decays and specific correction factors are applied. Once the amount of radioactivity measured in the container is quantified, the amount of the original intake can be estimated through applying radionuclide and intake pathway biokinetic models. The amount of the original intake is expressed as the radiation dose that will be delivered to that individual over the subsequent 50-year period (i.e., committed effective dose).

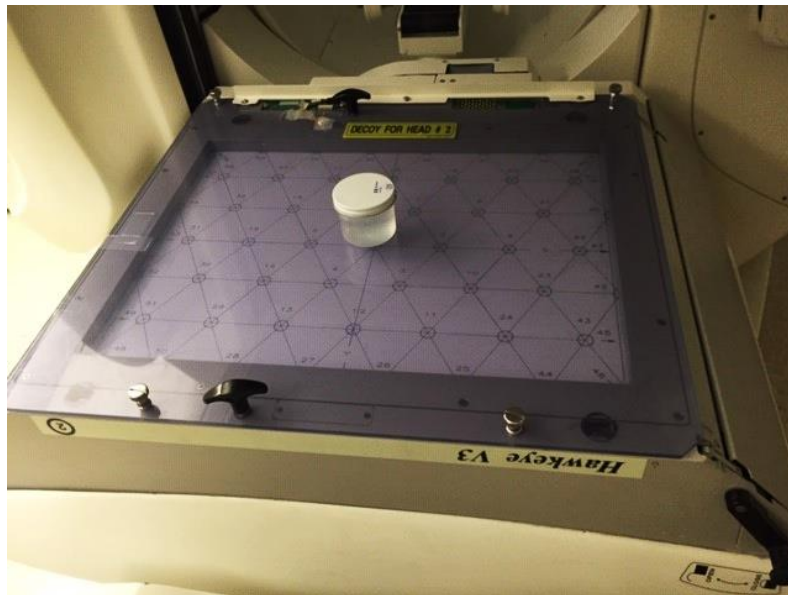


Figure 12 – Image of a urine specimen container placed on a General Electric Hawkeye V3 Gamma Camera detector

[Gamma Camera settings/protocol](#)

As previously discussed, the gamma camera is equipped with two detector heads with the detection surface area parallel to one another. One detector was oriented horizontally with the detector facing up so that the specimen container could be placed onto the detector as shown in Figure 12. To detect low amounts of radioactivity, collimators were removed from a General Electric Hawkeye gamma camera to prevent the effect they produce on reducing detection efficiency. For the detector to operate, a clear Lucite sheet with associated electronics must be inserted in place of a collimator so the electronics recognized that a collimator was not being used.

Posterior imaging was used for counting using a 256 x 256 pixel matrix, 1.23 magnification and a 10% energy window centered on the 140 keV peak for Tc-99m. The Exceleris software package provided by GE with the gamma camera was used to process and analyze the image data.

[Detector response to background radiation](#)

A three-minute background measurement was performed to determine the total contribution of background radiation to the signal. A urine specimen container filled with water to the 100 ml mark was placed on the center of detector 2 and the three-minute count initiated to obtain the background count rate. The background count rate was determined for a unit region-of-interest that could be reproduced in size and position on the display for subsequent counts. Background counts accumulated during the counting period were provided by the software for each region-of-interest.

Effect of sample volume on detector response

The urine specimen container can be modeled as a right cylindrical volume containing a homogeneous concentration of a radionuclide in a liquid medium. The detector response is a function of the height of the liquid column, i.e., as the column increases in height, radiation emitted in the direction of the detector in the upper layers of the liquid column must pass through a greater thickness of the liquid thus, resulting in the attenuation of more photons as compared to layers closest to the detector. In addition, as the column height increases, fewer photons are emitted in the direction of the region of interest on the detector.

The contribution of photons reaching the detector as a function of height in the liquid medium column was determined by MCNP using the energy of the emitted photon for the radionuclides of interest and the corresponding linear attenuation coefficient and build up as a function of material thickness. Figure 13 presents a diagram showing the height of the liquid column's effect on the angular response. (Chilton, Shultis, & Faw, 1984)

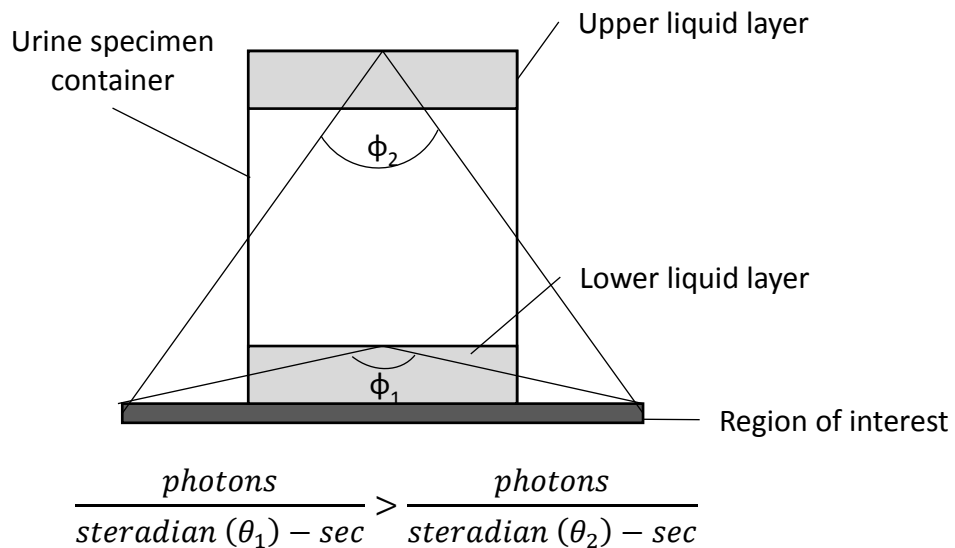


Figure 13: Detector response as a function of liquid column height

Gamma camera detector efficiency.

The NaI detector efficiency is photon energy dependent because the photoelectric effect dictates that lower energy photons are more likely to interact with the detector molecules and produce a detection event as compared to higher energy photons. Therefore, the photon detection efficiency of gamma camera will need to be calibrated for its energy response. The isotope Tc-99m (E=140 keV) was used to measure the energy dependent response of the gamma camera detector. A urine sample container with a pre-measured activity of Tc-99m filled with 100 ml of water (as a surrogate for urine) was placed on the Lucite plastic sheet for Detector 2 and a one-minute count obtained. An approximate 10,000 mm² square-shaped region of interest (ROI) was drawn on the monitor where the specimen container was located. The total counts detected in the ROI were decay corrected from the beginning of the one-minute count to the time of assay of the Tc-99m added to the specimen container. The count was repeated three times and the average was calculated.

Activity corrections for decay were determined using the general decay equation:

$$A(t) = A_0 e^{-\lambda t} \quad (\text{Eq. 31})$$

Solving for A_0 :

$$A_0 = \frac{A(t)}{e^{-\lambda t}} \quad (\text{Eq. 32})$$

Where A_0 is the activity corrected to the time of assay, λ is the decay constant for the radionuclide, and t is the elapsed time between time of assay and time the count was initiated.

The efficiency was calculated using the following equation:

$$Efficiency \left(\frac{c}{Y} \right) = \frac{Count\ Rate \left(\frac{c}{s} \right)}{A \left(\frac{d}{s} \right) Y \left(\frac{Y}{a} \right)} \quad (Eq. 33)$$

The efficiency was determined for Tc-99m and compared to the MCNP calculated result to validate the MCNP model.

[Cross talk between regions of interest](#)

Counting multiple urine specimen containers concurrently on a single detector could cause photons emitted from one container to be detected into an adjacent container region (show an image of what you mean). The MCNP model was used to quantify the impact of crosstalk between adjacent containers and regions of interest for both the 3/8-inch and one-inch crystal for each of the radionuclides of interest.

[Monte Carlo Modeling](#)

The cylindrical volume source equations can be used to calculate the gamma camera detector response from the urine specimen container, but the presence of an attenuating medium, i.e., the urine, causes the formulation to be more complicated. The formulation must be expressed analytically in terms of a geometrically elaborate integral requiring solution by numerical techniques. For this reason, the container and gamma camera detector were modeled using the Monte Carlo processing software MCNP v 6.0. The model was validated using radionuclides generally available in any nuclear medicine department. Once the MCNP model was validated, it was then used to calculate detector response to each of the radionuclides of interest.

MCNP was also used to calculate the detection efficiency of a one-inch thick sodium-iodide crystal for each of the radionuclides of interest. The activity concentration for each

radionuclide was held constant, as was the urine specimen container geometry, and energy windows for the radionuclides and the detector efficiency calculated. Detector efficiency is expected to increase with the one-inch thick NaI crystal.

Minimum Detectable Dose

The standard nuclear medicine gamma camera (model # and manufacturer) was used to measure the concentration of specific radionuclides in urine at levels to determine whether they meet the committed effective dose-based clinical decision guidelines.

To achieve this, background levels of radiation detected by a gamma camera, and its efficiency to detect the photons emitted by the radionuclides of interest were determined.

This allowed the calculation of the Minimum Detectable Dose (MDD) for comparison to the clinical decision guideline dose levels.

The minimum detectable dose is calculated using empirically derived Minimum Detectable Intake (MDI) equation (Anigstein, Olsher, & Loomis, 2010):

$$MDI (Bq) = \left(\frac{2.71 + 4.65\sqrt{B_{ROI}}}{Y_n \left(\frac{\lambda}{d}\right) E_n \left(\frac{c}{\bar{v}}\right) \left(\frac{V_s(ml)}{1400ml}\right)} \right) \quad (\text{Eq. 34})$$

Where B_{ROI} is the background counts in the region of interest, Y_n is the photon yield of energy E_i , and E_n is the efficiency of the detector for the n^{th} radionuclide of interest, and V_s is the volume of urine in the specimen container. (Anigstein, Olsher, & Loomis, 2010)

$$MDD (Sv) = MDI(Bq) \times UEF \left(\frac{Sv}{Bq} \right) \quad (\text{Eq. 35})$$

To obtain the MDD, the MDI is multiplied by the radionuclide's UEF (Sv/Bq) at time t . Each UEF is a function of the chemical composition of the radioisotope and the route of entry. UEF

dose conversion coefficients are divided into three types, Type F, Type M and Type S. The types are based on the rapidity by which they are cleared from the body as compared to hypothetical elements of specific constant absorption rates.

Type M is assumed when information is not available to assign an appropriate absorption type. Type F material is used when the amount absorbed into blood 30 days after an acute intake is greater than the amount that would be absorbed with a constant rate of absorption with a 10-day half time. Similarly, a Type S material would be selected when the amount absorbed into blood after 180 days after an acute intake is less than the amount that would be absorbed for a material with a constant rate of absorption into blood with a half time of 700 days.

III. Results

Background Determination

The GE Hawkeye V3 Gamma Camera is a dual head design with a 9.5 mm thick NaI crystal with an active area dimension of 60 cm x 45.7 cm. The camera is equipped with 59 photomultiplier tubes and includes software which allows for 4 discrete energy windows that can be set. The uniformity of the detector surface response is checked daily using a cobalt-57 flood source that covers the entire detector surface area. Corrections are made by adjusting the voltage applied to each individual photomultiplier tube to achieve a coefficient of variation less than $\pm 5\%$ across the surface of the detector.

A protocol was selected for use in counting background and sample counts that allowed for a window to be easily set around the desired energy peak and the count time set manually.

Four three-minute background counts were performed with the energy window set on 140 keV \pm 10%, and 5 distinct regions of the same pixel size on the detector surface were measured. The array of the ROI drawn on the monitor is shown in Figure 14.

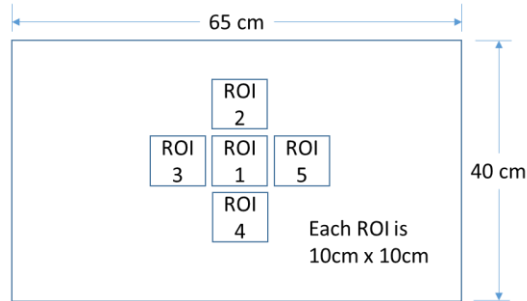


Figure 14: ROI array for background determination

Table 5 presents the counting results for background for the defined regions of interest.

Table 5: ROI Background Measurement

ROI #	Measurement 1 C _{ROI} in 3 min	Measurement 2 C _{ROI} in 3 min	Measurement 3 C _{ROI} in 3 min	Measurement 4 C _{ROI} in 3 min	Average (SD%)
1	2589	2984	2653	2956	2796 (6)
2	2520	2954	2660	2995	2782 (7)
3	2723	3306	2682	3272	2996 (10)
4	2570	3091	2716	3061	2856 (8)
5	2349	2685	2408	2658	2525 (6)
				Overall	2792 (7)

Each ROI was approximately 10,000 mm² and the count time was 3 minutes. The average count in the ROI was 15.5 counts per second per 10,000 mm² for an energy window of 140 keV \pm 10%.

Technitium-99m Validation of MCNP Model

The specification for Tc-99m are presented in Table 6. Table 7 presents the measurements results and efficiency of the gamma camera to detect the 140 keV gamma ray.

Table 6: Specifications for Tc-99m

Tc-99m half-life	6.007 hours
Activity measured at t=0	10.23 μ Ci (378,510 d/s)
Energy Window	140 keV \pm 10%
Decay constant for Tc-99m	0.0019 min ⁻¹
Tc-99m γ yield at 141 keV	0.89 γ /d

Table 7: Tc-99m Activity Measurements in ROI

ROI 1	Time of count	C _{ROI}		Elapsed time		Correction factor	Corrected Activity	Counts per sec
1	15:26	2229770	c/m	1.00	min	0.99807868	2234062	37234
2	15:31	2272968	c/m	6.00	min	0.98852734	2299348	38322
3	16:05	2057220	c/m	40.00	min	0.92595786	2221721	37028
							Average	37528

The efficiency of the detector Tc-99m at 140 keV \pm 10% for a 100 ml urine specimen geometry was:

$$Efficiency \left(\frac{c}{\gamma} \right) = \frac{Count\ Rate \left(\frac{c}{s} \right)}{A \left(\frac{d}{s} \right) Y \left(\frac{\gamma}{d} \right)} = \frac{37528 - 15}{(378,510)(0.89)} = 0.111 \frac{c}{\gamma} \text{ or } 11.1\%$$

The detector efficiency for the urine specimen geometry on the Hawkeye Gamma Camera was modeled in MCNP using the parameters in Table 8.

Table 8: MCNP Input Parameters for comparison to experimental results

Input parameter	Value
Urine vol. (ml)	100

Activity (Bq)	1
Energy window (keV)	126 – 156
Detector thickness (mm)	10
Acrylic cover thickness (mm)	6
Detector size (mm)	400 x 400
Region of Interest size (mm)	100 x 100
Air gap from cover to detector (mm)	20
# of histories	1x10 ⁷

The efficiency for Tc-99m using MCNP for the given input parameters was calculated as 12.0%. The difference between experimental and theoretical efficiencies was:

$$\frac{11.1\% - 12.0\%}{12.0\%} = \pm 8\%$$

[MCNP derived efficiencies for radionuclides of interest](#)

MCNP was used to calculate the efficiency of the Hawkeye Gamma Camera and urine specimen sample container geometry as a function of photon energy. Table 9 and Figure 15 present the results of the MCNP model for both the 3/8-inch (1 cm) NaI crystal and a one-inch (2.54 cm) crystal, respectively.

Table 9: Detector efficiencies for photon energy ranges from 75 keV to 1400 keV

Energy (MeV)	Energy (keV)	3/8-inch (1 cm) Thick crystal	1-inch (2.54 cm) Thick crystal
0.0750	75	12.6%	12.6%
0.1000	100	12.8%	12.9%
0.1250	125	12.5%	12.8%
0.1500	150	11.5%	12.5%
0.1750	175	10.1%	12.0%
0.2000	200	8.7%	11.4%
0.2250	225	7.4%	10.6%
0.2500	250	6.3%	9.7%
0.2750	275	5.4%	8.9%
0.3000	300	4.7%	8.2%
0.3250	325	4.1%	7.5%
0.3500	350	3.6%	6.9%
0.3750	375	3.2%	6.4%
0.4000	400	2.9%	5.9%
0.4250	425	2.6%	5.5%
0.4500	450	2.4%	5.1%
0.4750	475	2.2%	4.8%
0.5000	500	2.0%	4.5%
0.5500	550	1.7%	4.1%
0.6000	600	1.5%	3.7%
0.6500	650	1.3%	3.4%
0.7000	700	1.2%	3.1%
0.7500	750	1.1%	2.9%
0.8000	800	1.0%	2.7%
0.8500	850	0.9%	2.5%
0.9000	900	0.9%	2.4%
0.9500	950	0.8%	2.2%
1.0000	1000	0.8%	2.1%
1.0500	1050	0.7%	2.0%
1.1000	1100	0.7%	1.9%
1.1500	1150	0.6%	1.9%
1.2000	1200	0.6%	1.8%
1.2500	1250	0.6%	1.7%
1.3000	1300	0.5%	1.6%
1.3500	1350	0.5%	1.6%
1.4000	1400	0.5%	1.5%

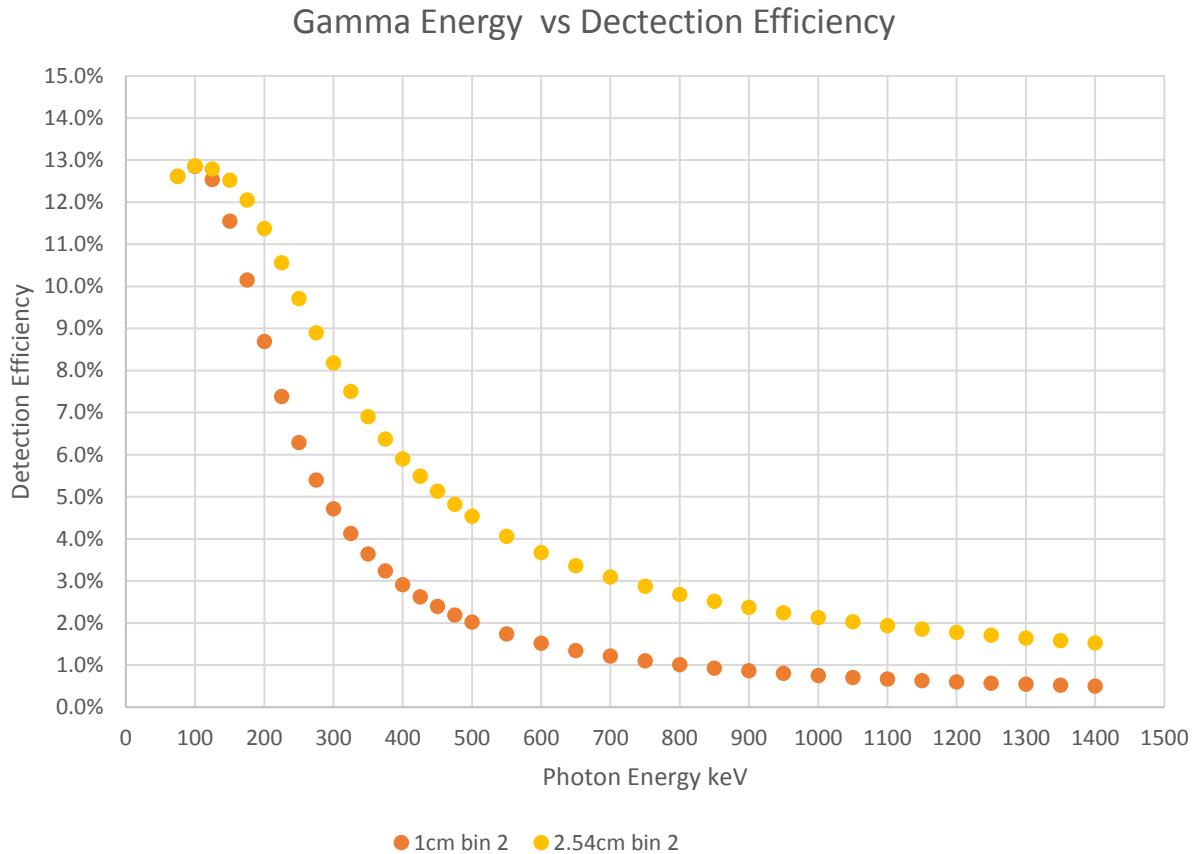


Figure 15: Gamma Energy versus MCNP-derived Detection Efficiency for the 3/8-inch (1 cm) and one-inch (2.54 cm) NaI crystal

Table 10 presents the detector efficiency for the radionuclides of interest determined using the MCNP model for the Hawkeye Gamma Camera (1 cm crystal thickness) and 100 ml urine specimen geometry.

Table 10: MCNP-derived efficiencies for Radionuclides of Interest for a 1 cm thick NaI crystal

Radionuclide	Energy Range (Peak keV $\pm 10\%$)	Efficiency (%)
Cobalt-60	1056 - 1466	0.8
Iodine-131	328 - 401	2.9
Cesium-137	595 - 728	1.4
Iridium-192	267 - 348	3.1

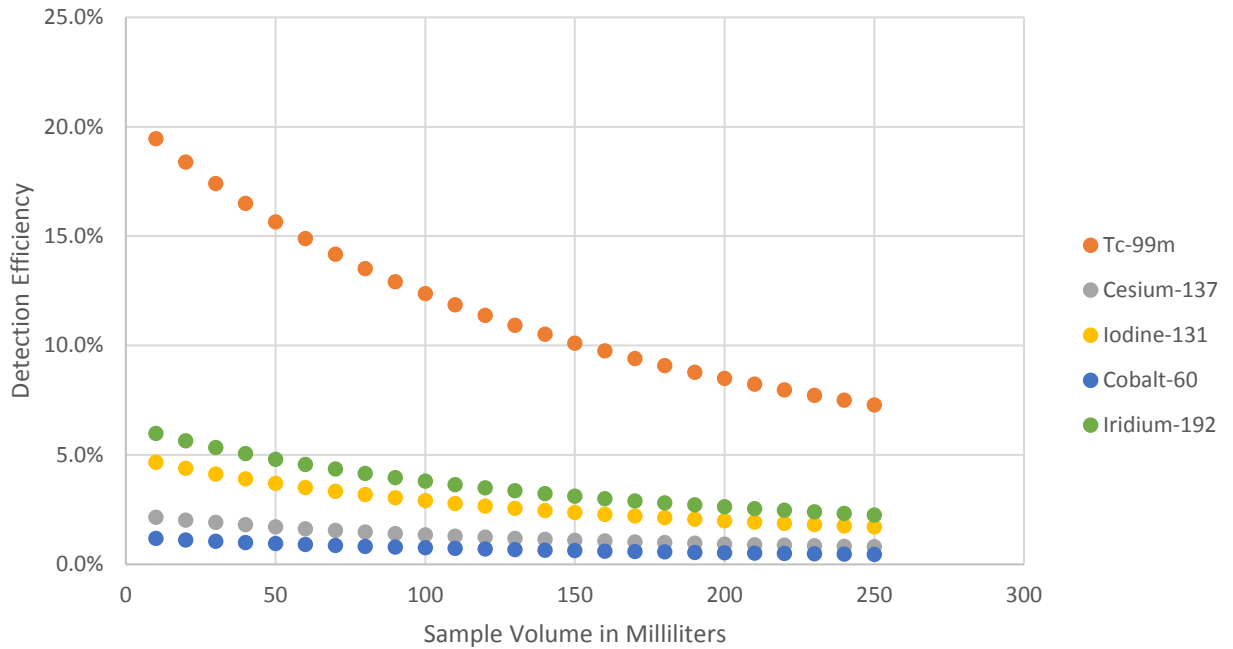


Figure 16: Detection Efficiency vs Sample Size for 1 cm NaI Crystal

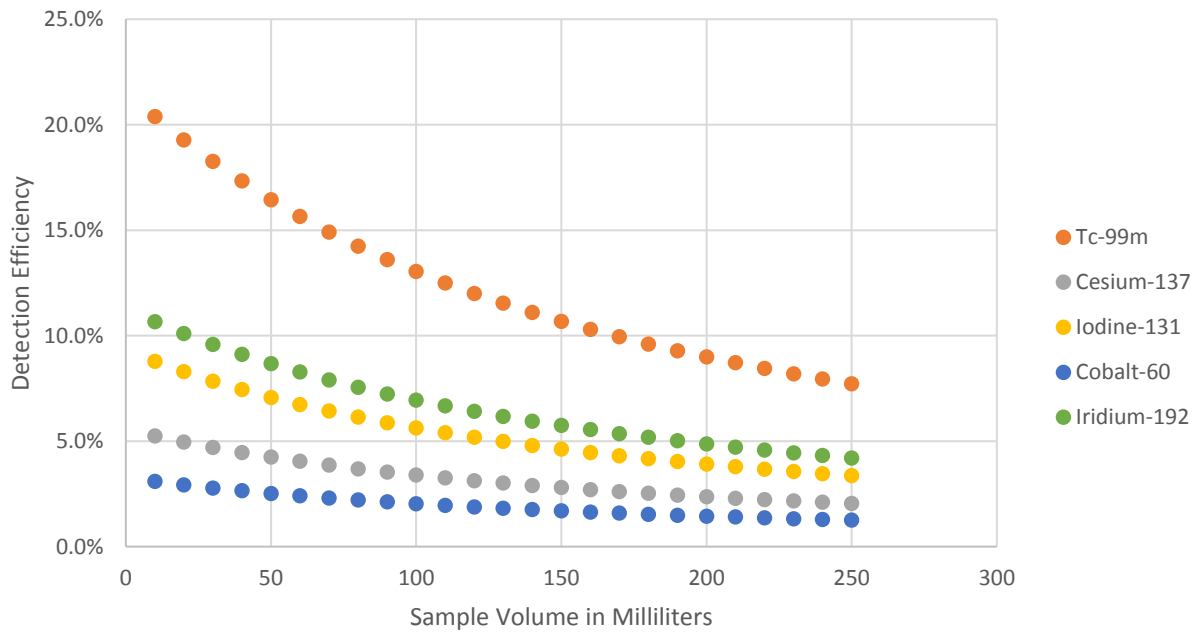


Figure 17: Detection Efficiency vs Sample Size for 2.54 cm NaI Crystal

Table 11 presents detector efficiency for radionuclides of interest with specified energy windows at increasing urine volume from 10 ml to 250 ml for a 3/8-inch (1 cm) and 1-inch (2.54 cm) thick NaI crystal.

Table 11: Calculated detector efficiency for radionuclides of interest with energy windows as a function of urine sample volume for a one-inch (2.54 cm) thick NaI crystal

Vol. (ml)	(1056-1466 keV)		(126 - 156 keV)		(328 - 401 keV)		(595 - 728 keV)		(267 -348 keV)	
	Cobalt-60		Tc-99m		Iodine-131		Cesium-137		Iridium-192	
	1 cm	2.54 cm	1 cm	2.54 cm	1 cm	2.54 cm	1 cm	2.54 cm	1 cm	2.54 cm
10	1.2%	3.1%	19.5%	20.4%	4.7%	8.8%	2.2%	5.2%	4.9%	8.4%
20	1.1%	2.9%	18.4%	19.3%	4.4%	8.3%	2.0%	5.0%	4.7%	8.0%
30	1.1%	2.8%	17.4%	18.3%	4.1%	7.8%	1.9%	4.7%	4.4%	7.6%
40	1.0%	2.6%	16.5%	17.3%	3.9%	7.4%	1.8%	4.5%	4.2%	7.2%
50	1.0%	2.5%	15.7%	16.4%	3.7%	7.1%	1.7%	4.2%	4.0%	6.8%
60	0.9%	2.4%	14.9%	15.6%	3.5%	6.7%	1.6%	4.0%	3.8%	6.5%
70	0.9%	2.3%	14.2%	14.9%	3.3%	6.4%	1.6%	3.9%	3.6%	6.2%
80	0.8%	2.2%	13.5%	14.2%	3.2%	6.1%	1.5%	3.7%	3.4%	6.0%
90	0.8%	2.1%	12.9%	13.6%	3.0%	5.9%	1.4%	3.5%	3.3%	5.7%
100	0.8%	2.0%	12.4%	13.0%	2.9%	5.6%	1.4%	3.4%	3.1%	5.5%
110	0.7%	2.0%	11.9%	12.5%	2.8%	5.4%	1.3%	3.2%	3.0%	5.3%
120	0.7%	1.9%	11.4%	12.0%	2.7%	5.2%	1.2%	3.1%	2.9%	5.1%
130	0.7%	1.8%	10.9%	11.5%	2.6%	5.0%	1.2%	3.0%	2.8%	4.9%
140	0.7%	1.7%	10.5%	11.1%	2.5%	4.8%	1.1%	2.9%	2.7%	4.7%
150	0.6%	1.7%	10.1%	10.7%	2.4%	4.6%	1.1%	2.8%	2.6%	4.5%
160	0.6%	1.6%	9.8%	10.3%	2.3%	4.5%	1.1%	2.7%	2.5%	4.4%
170	0.6%	1.6%	9.4%	9.9%	2.2%	4.3%	1.0%	2.6%	2.4%	4.2%
180	0.6%	1.5%	9.1%	9.6%	2.1%	4.2%	1.0%	2.5%	2.3%	4.1%
190	0.6%	1.5%	8.8%	9.3%	2.1%	4.0%	1.0%	2.4%	2.2%	4.0%
200	0.5%	1.4%	8.5%	9.0%	2.0%	3.9%	0.9%	2.4%	2.2%	3.8%
210	0.5%	1.4%	8.2%	8.7%	1.9%	3.8%	0.9%	2.3%	2.1%	3.7%
220	0.5%	1.4%	8.0%	8.4%	1.9%	3.7%	0.9%	2.2%	2.0%	3.6%
230	0.5%	1.3%	7.7%	8.2%	1.8%	3.6%	0.8%	2.2%	2.0%	3.5%
240	0.5%	1.3%	7.5%	7.9%	1.8%	3.5%	0.8%	2.1%	1.9%	3.4%
250	0.5%	1.3%	7.3%	7.7%	1.7%	3.4%	0.8%	2.0%	1.9%	3.3%

Crosstalk between adjacent regions of interest

The cross talk from one ROI to another for the fixed sample geometry was calculated for each radionuclide of interest using MCNP v6.0. The positioning of ROI A with respect to ROI B is presented in Figure 18. The results are presented in Figures 19 through 22. The concentration of activity was held constant, the ROI area is defined as 10 cm x 10 cm, and the solution volume varied from 30, 60, to 90 ml. The cross talk between regions of interest was also calculated as the distance between them ranged from 0 cm (touching) to 19.5 cm for the 3/8-inch and one-inch NaI crystals. The results are presented for each radionuclide in Figures 21 through 25.

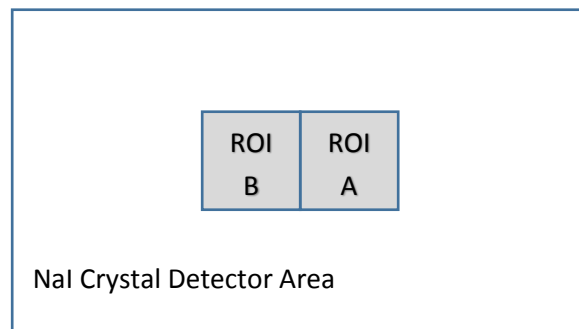


Figure 18: Detector active surface area with ROI

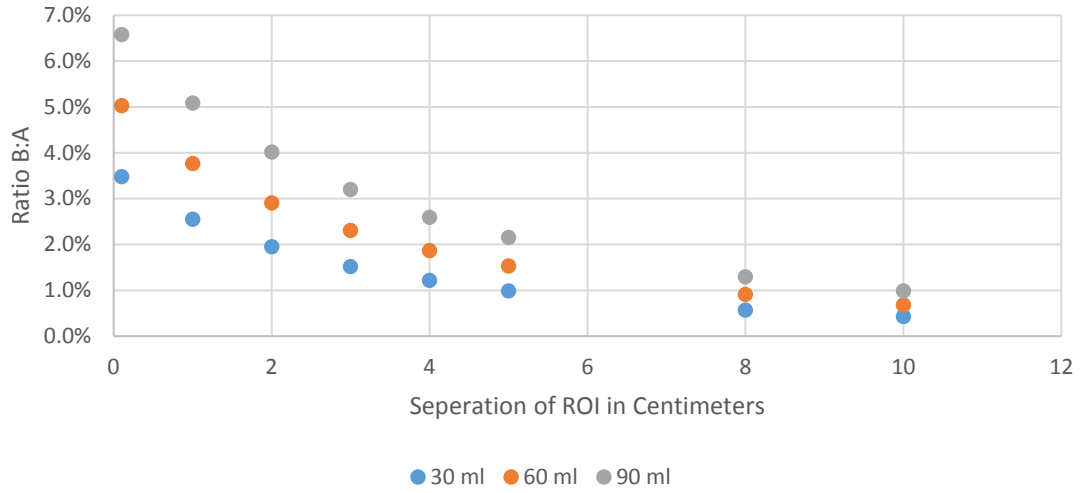


Figure 19: Tc-99m Percent Count in ROI B from Sample in ROI A for Sample volume of 30, 60 and 90 ml

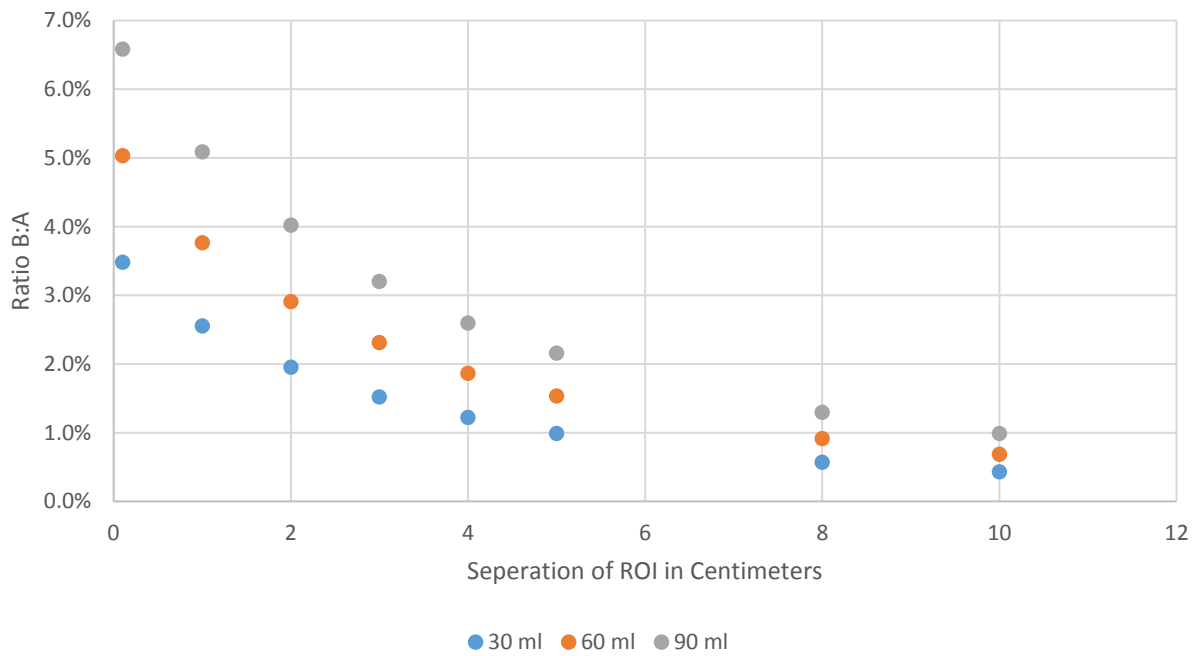


Figure 20: Tc-99m Percent Count in ROI B from Sample in ROI A for volume of 30, 60 and 90 ml

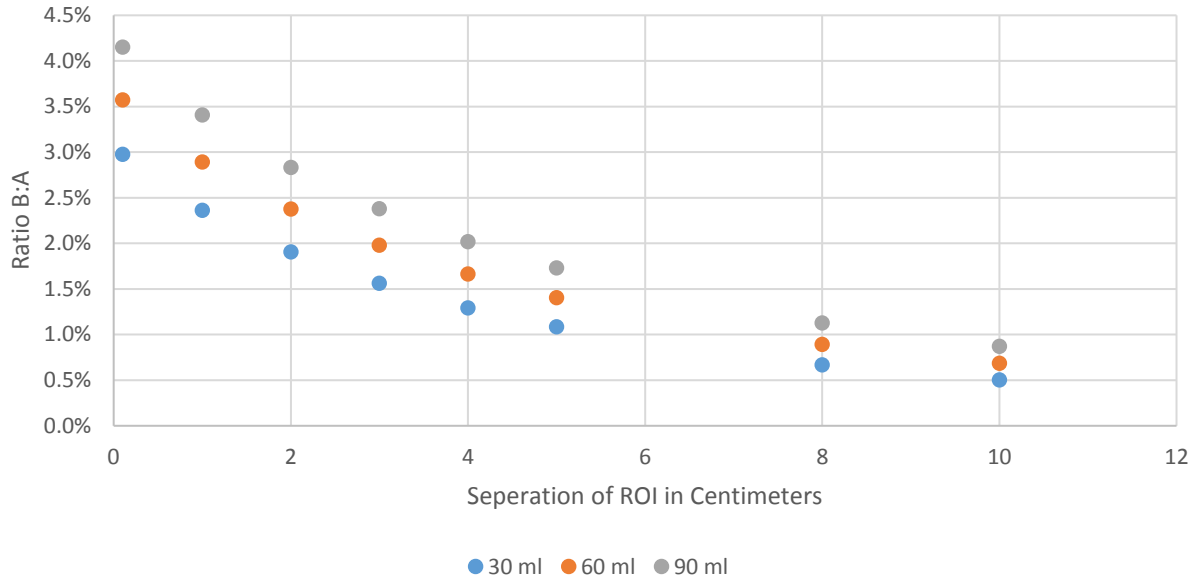


Figure 21: Cs-137 Percent Count in ROI B from Sample in ROI A for volume of 30, 60 and 90 ml

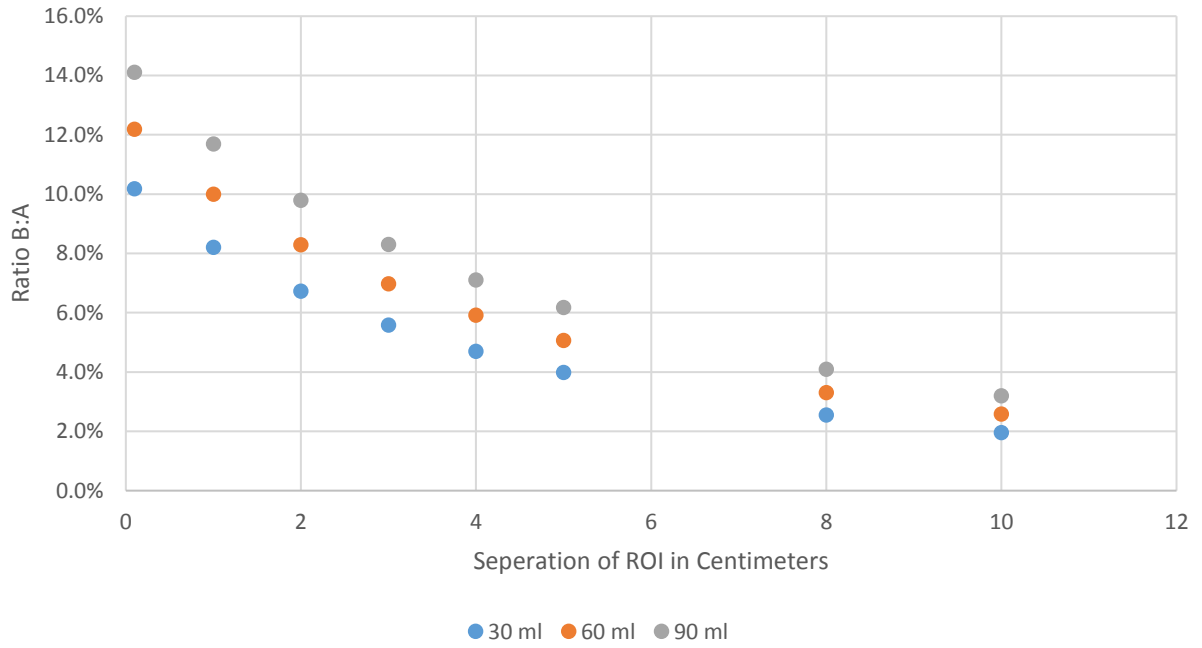


Figure 22: Cobalt-60 Percent Count in ROI B from Sample in ROI A for volume of 30, 60 and 90 ml

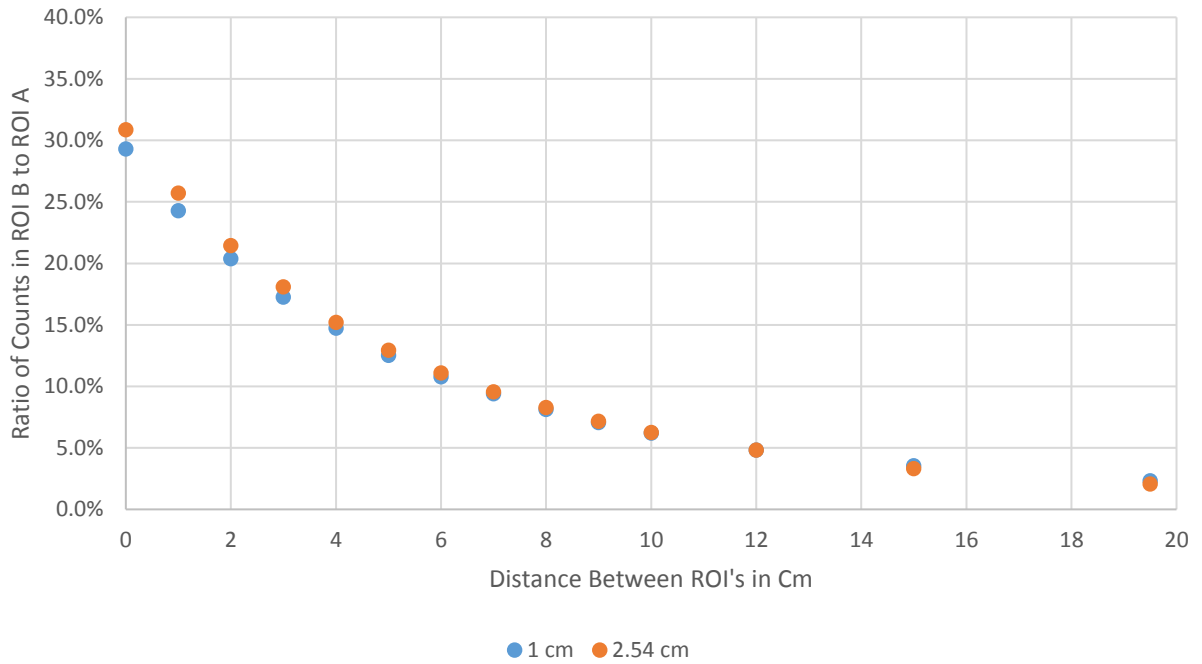


Figure 23: Cobalt-60 Crosstalk (%) for Separation Distances of ROI's from 0 - 19.5 cm

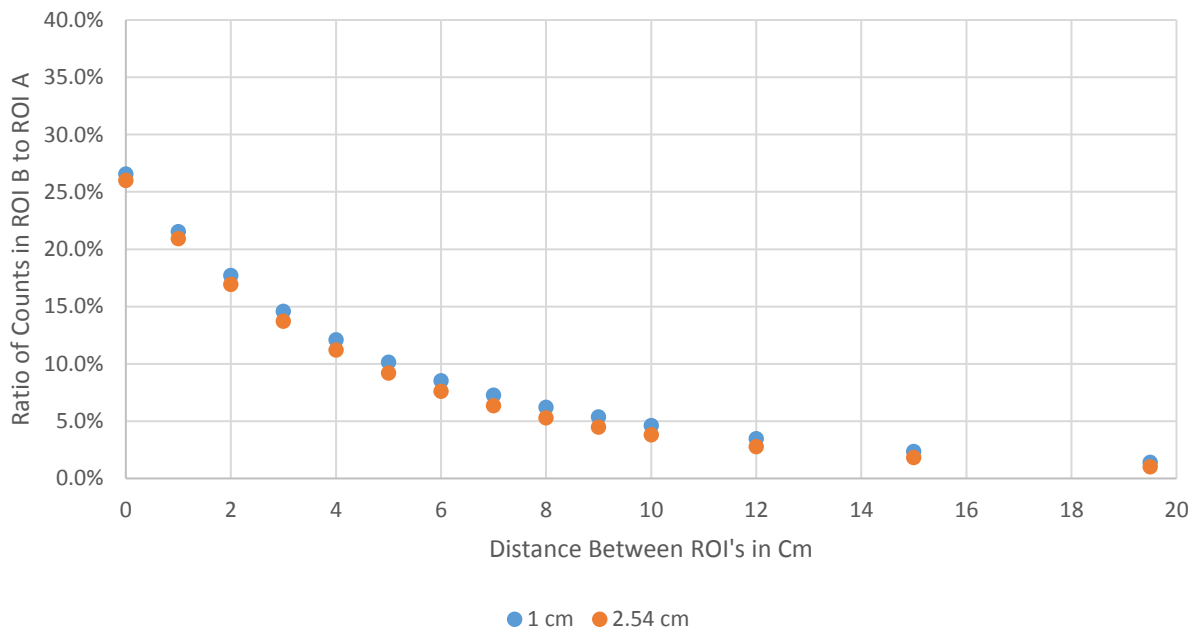


Figure 24: Iodine-131 Crosstalk for Separation Distances of ROI's for Separation from 0 - 19.5 cm

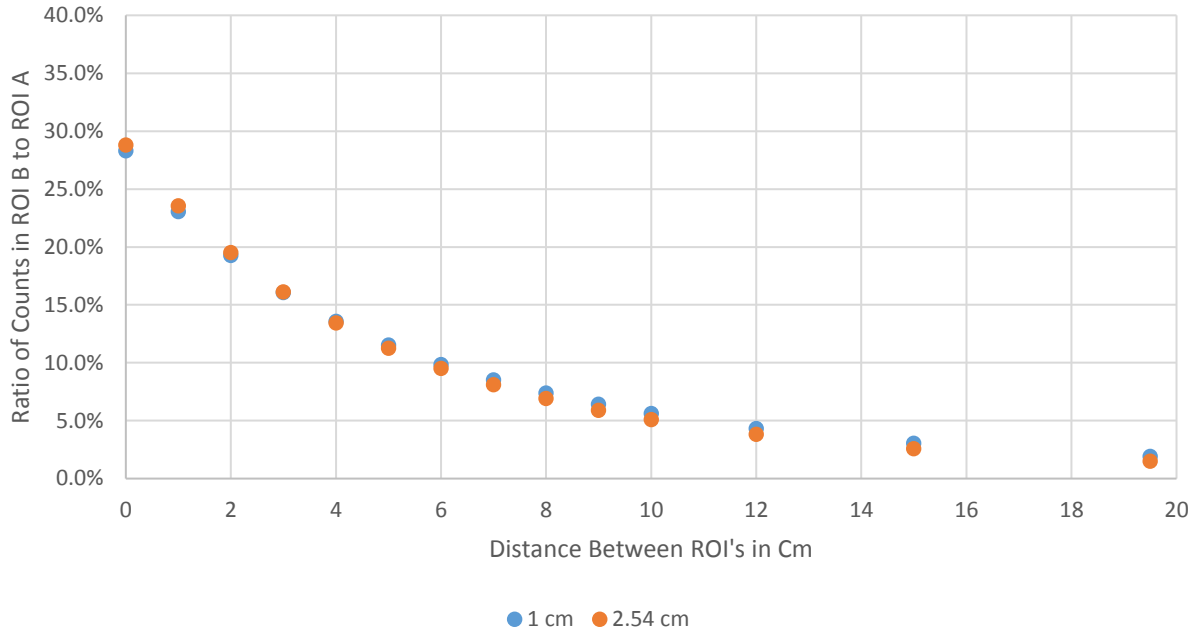


Figure 25: Cesium-137/Barium-137m Crosstalk (%) for Separation Distances of ROI's from 0 - 19.5 cm

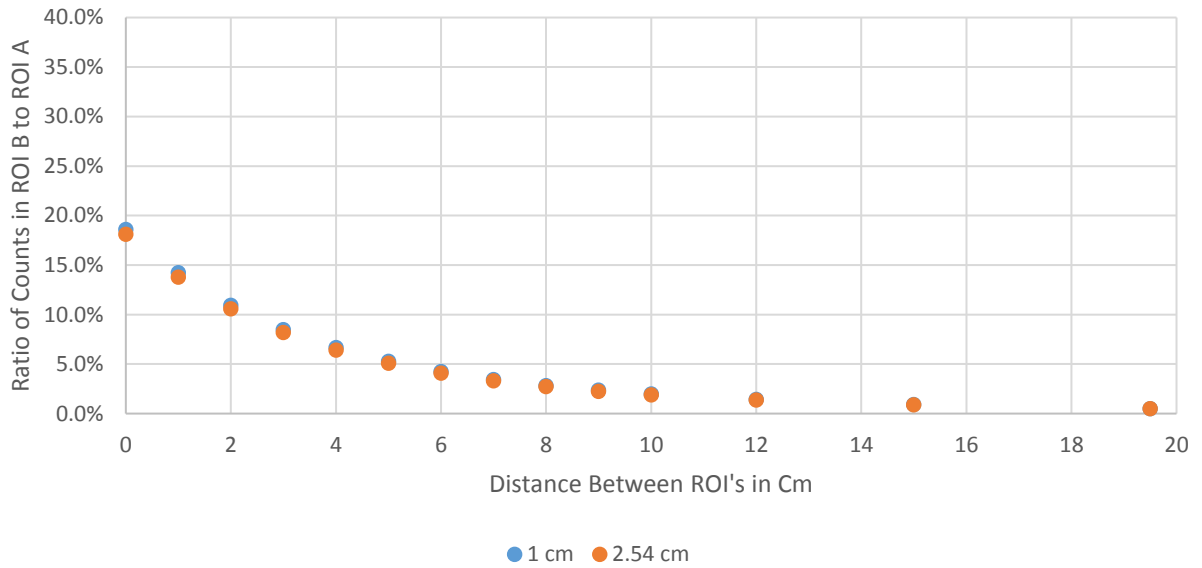


Figure 26: Technitium-99m Crosstalk for Separation Distances of ROI's from 0 - 19.5 cm

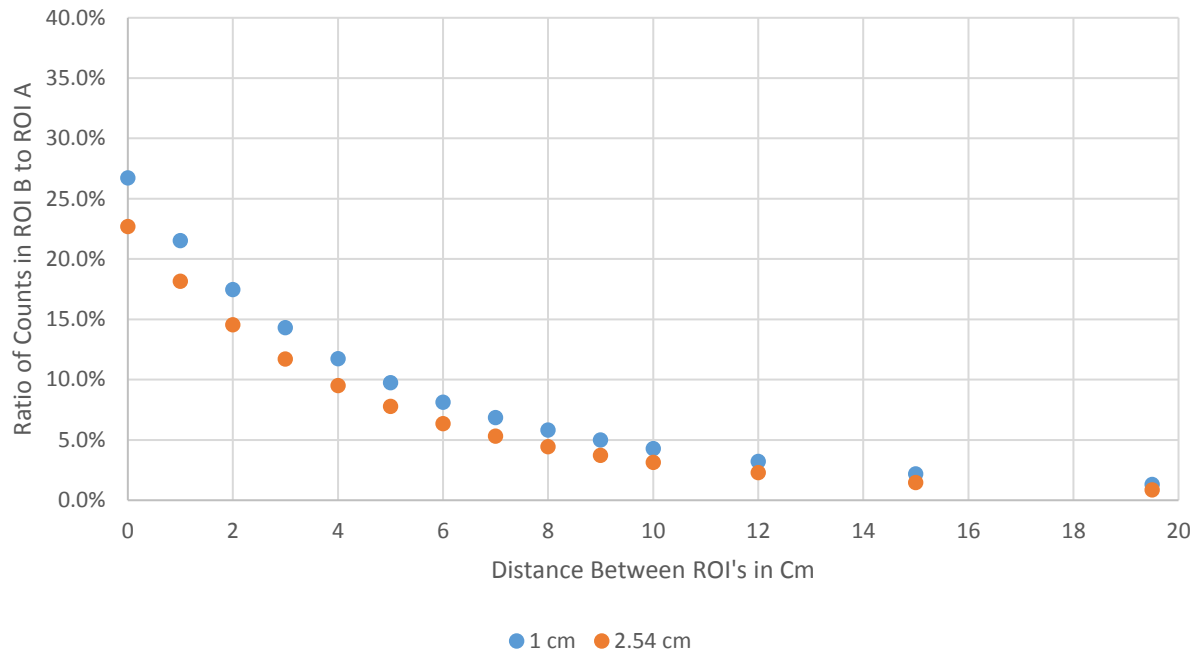


Figure 27: Iridium-192 Crosstalk (%) for Separation Distances of ROI's from 0 - 19.5 cm

Minimum Detectable Intake

The MDI is calculated using the following equation which is based on the background count rate in the region of interest:

$$MDI (Bq) = \left(\frac{2.71 + 4.65\sqrt{B_{ROI}}}{Y_n \left(\frac{\gamma}{d}\right) E_n \left(\frac{c}{\gamma}\right) \left(\frac{V_S(ml)}{1400ml}\right)} \right) \text{ (Eq. 8)}$$

The background counts in the region of interest for different energy windows selected on the gamma camera and the average was presented in Table 5. The background radiation measurements for the gamma camera at specific energies using three regions of interest of similar size are presented in Table 12.

Table 12: Background measurements at select gamma energy windows.

Energy Window (keV)	Energy peak center (keV)	Measurement 1 C _{ROI} in 3 min	Measurement 2 C _{ROI} in 3 min	Measurement 3 C _{ROI} in 3 min	Average (Counts/sec) (SD%)
45 - 55	50	1410	1579	2513*	8.3 (8)
90 - 110	100	19745*	10988	11698	63 (4)
135 - 165	150	3467	3492	4218	20.7 (11)
225 - 275	250	2516	2492	2551	14.0 (1)
364	364	1408	1441	1440	7.9 (1)

* Background value affected by patient being scanned in adjacent room. Data point not used to calculate average.

The distribution of background counts as a function of energy for the GE Hawkeye Gamma Camera is presented in Figure 28.

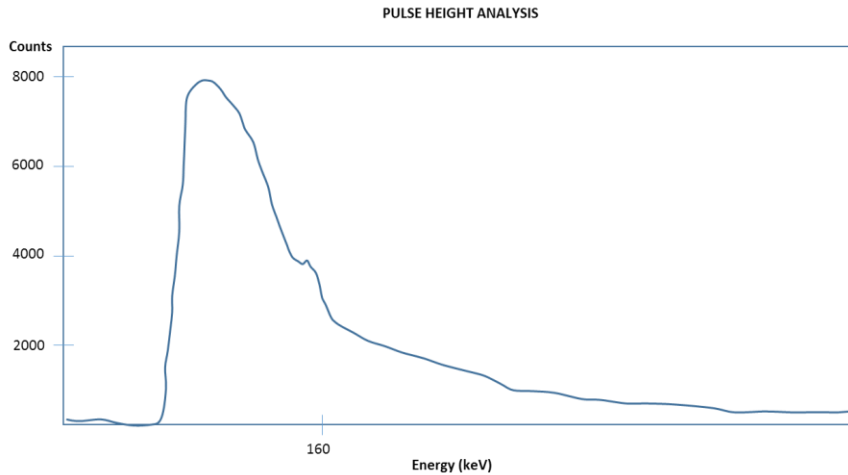


Figure 28: Background photon energy distribution for the GE Hawkeye V3, 3/8-inch NaI crystal

Table 13 presents the data for the Radionuclides of Interest used to calculate the MDI, the MCNP-derived efficiency, photon yield, value of the background detection events at the

radionuclide energy and the resulting MDI. All values are for a sample of 100 ml and a 1 cm thick NaI crystal.

Table 13: MDI and calculation parameters for the radionuclides of interest at 100 ml and 1 cm thick NaI crystal

Radio-nuclide	Energy (keV)	Efficiency (c/γ)	Yield (γ/d)	Background (c/s)	MDI (Bq)
Co-60	1025	0.008	2	7.9	13807
I-131	364	0.029	0.815	7.9	9347
Cs-137	662	0.014	0.851	7.9	18543
Ir-192	316	0.031	0.82	10	9591

Minimum detectable dose (MDD)

Minimum detectable dose (MDD) for a 100 ml sample at time *t* post incident was calculated by multiplying the MDI by the UEF (Sv/Bq). The results of the MDD calculations are presented in Tables 14 through 17.

$$MDD (Sv) = MDI(Bq) \times UEF \left(\frac{Sv}{Bq} \right) \text{ (Eq. 9)}$$

Table 14: MDD for cobalt-60 (t) days post incident for a 100 ml sample

Cobalt-60 MDD (Sv)			
Days	Type F	Type M	Type S
1	1.79E-03	1.28E-02	1.28E+00
2	4.28E-03	3.04E-02	3.04E+00
3	7.59E-03	5.25E-02	5.38E+00
4	1.12E-02	7.32E-02	7.59E+00
5	1.52E-02	9.53E-02	1.01E+01
6	1.93E-02	1.17E-01	1.27E+01
7	2.35E-02	1.38E-01	1.52E+01
8	2.90E-02	1.66E-01	1.79E+01
9	3.59E-02	1.93E-01	2.21E+01
10	4.14E-02	2.07E-01	2.49E+01
15	7.59E-02	3.04E-01	3.87E+01
30	2.07E-01	4.97E-01	7.04E+01
45	4.14E-01	6.35E-01	9.11E+01

60	6.63E-01	7.32E-01	1.04E+02
90	1.09E+00	9.11E-01	1.17E+02
180	2.49E+00	1.66E+00	1.52E+02
365	6.35E+00	4.83E+00	2.07E+02

Table 15: MDD for iodine-131 (t) days post incident for a 100 ml sample

Iodine-131 MDD (Sv)			
Days	Type F	Type M	Type S
1	2.71E-04	3.64E-04	1.69E-03
2	1.36E-03	1.10E-03	4.57E-03
3	1.02E-02	7.62E-03	3.22E-02
4	8.05E-02	4.07E-02	1.86E-01
5	3.39E-01	9.32E-02	4.66E-01
6	4.91E-01	1.19E-01	6.35E-01
7	4.83E-01	1.36E-01	7.37E-01
8	4.66E-01	1.52E-01	8.22E-01
9	4.57E-01	1.69E-01	9.32E-01
10	4.66E-01	1.86E-01	1.02E+00
15	5.59E-01	2.88E-01	1.61E+00
30	1.69E+00	1.02E+00	5.68E+00
45	6.52E+00	4.07E+00	2.12E+01
60	2.54E+01	1.61E+01	8.22E+01
90	4.07E+02	2.54E+02	1.19E+03

Table 16: MDD for cesium-137 (t) days post incident for a 100 ml sample

Cesium-137 MDD (Sv)			
Days	Type F	Type M	Type S
1	6.79E-03	2.40E-02	1.20E+00
2	1.44E-02	3.79E-02	1.88E+00
3	2.20E-02	6.19E-02	3.00E+00
4	3.00E-02	8.39E-02	4.19E+00
5	3.39E-02	9.98E-02	4.99E+00
6	3.79E-02	1.12E-01	5.59E+00
7	4.19E-02	1.22E-01	5.99E+00
8	4.59E-02	1.30E-01	6.39E+00
9	4.79E-02	1.36E-01	6.79E+00
10	4.79E-02	1.40E-01	6.99E+00
15	5.39E-02	1.54E-01	7.79E+00

30	6.19E-02	1.74E-01	8.79E+00
45	6.99E-02	1.94E-01	9.98E+00
60	7.99E-02	2.20E-01	1.10E+01
90	1.02E-01	2.60E-01	1.36E+01
180	2.20E-01	4.79E-01	2.40E+01
365	9.78E-01	1.74E+00	6.99E+01

Table 17: MDD for iridium-192 (t) days post incident for a 100 ml sample

Iridium-192 MDD (Sv)			
Days	F	M	S
1	3.80E-04	5.06E-03	1.45E-01
2	1.96E-03	2.15E-02	6.26E-01
3	3.10E-03	3.48E-02	1.08E+00
4	4.05E-03	4.43E-02	1.33E+00
5	5.00E-03	5.19E-02	1.64E+00
6	5.95E-03	5.95E-02	1.90E+00
7	6.96E-03	6.96E-02	2.15E+00
8	7.59E-03	6.96E-02	2.40E+00
9	8.86E-03	7.59E-02	2.59E+00
10	9.49E-03	8.22E-02	2.85E+00
15	1.39E-02	1.08E-01	3.80E+00
30	3.10E-02	1.71E-01	6.33E+00
45	5.06E-02	2.21E-01	8.86E+00
60	6.96E-02	2.78E-01	1.08E+01
90	1.20E-01	4.18E-01	1.52E+01
180	4.36E-01	1.33E+00	3.86E+01
365	4.74E+00	1.39E+01	2.59E+02

IV. Discussion

The results for the validation of the MCNP model demonstrated that the model was sufficiently accurate to calculate the efficiency of the Hawkeye gamma camera and urine specimen container geometry. MCNP calculated the detector efficiency as 12% as shown in Figure 25. Measurement of the detector efficiency was 11.1% for a difference of 8%. The

activity of Tc-99m (140 keV) was measured using the Capintec well counter; however, the measurement of 10.23 μCi of Tc-99m is the minimum of the calibrated range of the Capintec. Therefore, this contributed to the difference between the measured detector efficiency and MCNP calculated value. Each MCNP derived detection efficiency was based on 1×10^7 histories for an uncertainty of $<0.1\%$. Notwithstanding the likely inaccuracy in measured Tc-99m activity, the validation results are sufficiently accurate and the MCNP model is considered accurate. The model was used to calculate detector efficiencies for the 3/8-inch (1 cm) and one-inch (2.54 cm) thick NaI detectors.

For each radionuclide of interest, background values for the predominant photon energy window was used to calculate the Minimum Detectable Concentration (MDC), which was converted to Minimum Detectable Intake (MDI), and the Minimum Detectable Dose (MDD) for Types F, M and S materials. For the counting geometry, background values were measured for the energy windows at 50, 100, 150, 250 and 364 keV. This involved placing a urine specimen container holding 100 ml of water with no radioactivity introduced on the center of the detector, a three-minute count initiated, and a 10 cm x 10 cm ROI used to quantify the number of detection events expressed as counts per second. Background values are used to calculate MDI as described in Equation 8. These values were used in the MDC equation along with the MCNP derived efficiency for the predominant photon energy of the radionuclide of interest, with the volume normalized to 1.4 liters (reference person daily urinary excretion volume). The value was divided by the radionuclide specific urinary excretion fraction to determine the radionuclide intake and subsequent MDD, as a function of the time elapsed between the incident (i.e., intake) and the urine sample collection. If the

time elapsed between sample collection and analysis is a significant fraction of the radionuclide half-life, a decay correction calculation must be applied. The results for these calculations are described below.

Cobalt-60

Figure 27 shows for cobalt-60, the maximum time post incident that a committed dose of 20 mSv is detectable in urine specimens counted on the Hawkeye gamma camera is approximately 6 days for Type F, 1 day for Type M, and is undetectable for Type S. For a MDD of 250 mSv, the time post incident that a dose is detectable is 30 days for Type F, 10 days for Type M and is undetectable for Type S. Although the detection efficiency for the gamma camera is much lower due to the higher energy photons, the background is comparably less so a window established to detect photons with an average of 1025 keV can provide sufficient sensitivity to positively detect intakes resulting in a 20 mSv committed dose or less. The MDD was calculated based on a background value of 7.9 counts per second, determined for 364 keV, which is considered conservative based on the background spectrum versus photon energy displayed by the gamma camera software.

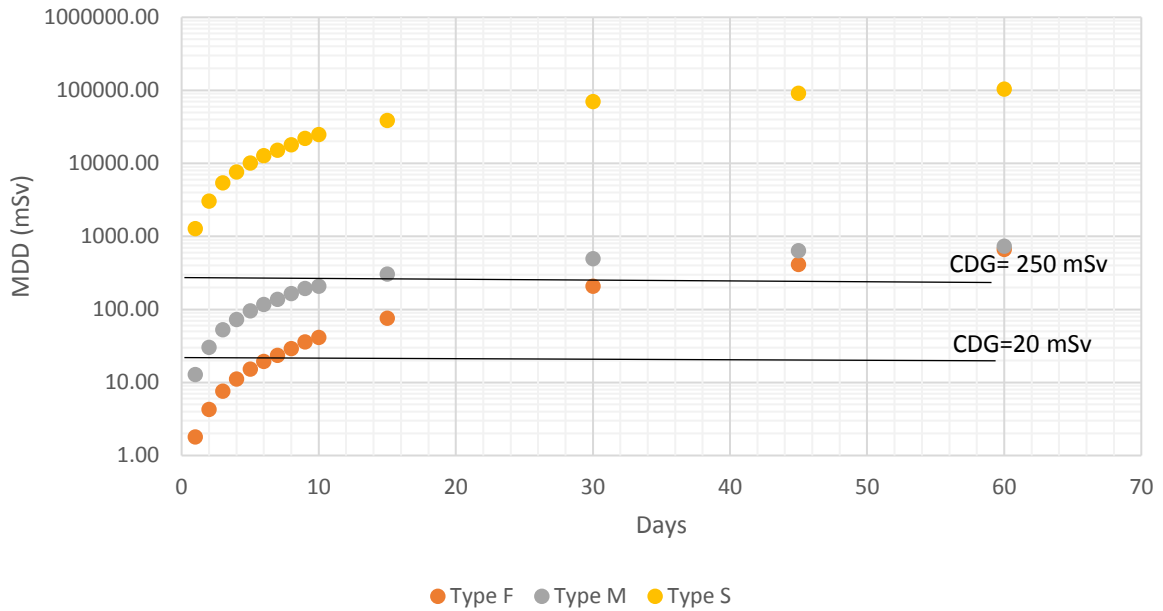


Figure 29: MDD for Cobalt-60 (Type F, S, M) days post incident

The detector efficiency as a function of urine sample volume containing Cobalt-60 (as presented in Table 11) assuming a constant concentration ranged from 1.2% for 10 ml sample volume to 0.5% for a 250 ml sample volume, and an efficiency of 0.7% for 100 ml for the 3/8-inch crystal. This resulted in a 35.3 % reduction for a sample volume of 100 ml. The reduced efficiency was due to self-attenuation of the photons in the sample as well as photon emissions from upper layers of the solution emitted in the direction of the detector falling outside the ROI. The one-inch crystal ranged from 3.1% for a 10 ml urine sample to 1.3% for a 250 ml sample, with 2% at 100 ml. This resulted in a 35% reduction for a sample volume of 100 ml. The difference in efficiency between the two crystals for the 100 ml sample is due to the higher detection efficiency for the 1025 keV photons in the one-inch crystal.

The contribution of counts from a urine sample in ROI 1 to the counts of a sample in ROI 2 was determined for separation distances ranging from 0 cm (ROIs touching) to 19.5 cm (as

presented in Figure 21). The contribution ranged from approximately 29.3% for ROIs that are immediately adjacent (touching) to 2.3% at a separation of 19.5 cm for the 3/8-inch crystal. The contribution ranged from approximately 30.9% for ROIs that are immediately adjacent (touching) to 2.1% at a separation of 19.5 cm for the one-inch crystal.

[Iodine-131](#)

Figure 28 shows for iodine-131 the maximum time post incident that a committed dose of 20 mSv is detectable in urine specimens counted on the Hawkeye gamma camera is approximately 3 days for Type F, 3 days for Type M, and 2 days for Type S. For a MDD of 250 mSv, the time post incident that a dose is detectable is 4 days for Type F, 10 days for Type M and 4 days for Type S. These values are consistent with known excretion of iodine-131 in urine. For a reference person, approximately 80% of iodine-131 as sodium iodide is excreted in urine within 48 hours. (ICRP, 2017)

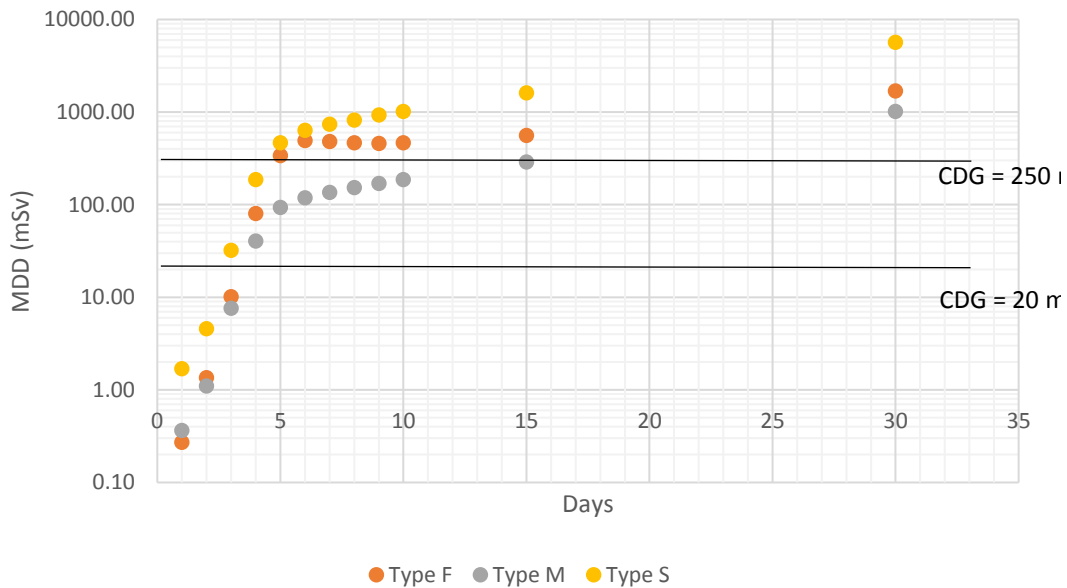


Figure 30: MDD for Iodine-131 (Type F, S, M) days post incident

The detector efficiency as a function of urine sample volume containing Iodine-131 (see Table 11) assuming a constant concentration ranged from 4.7% for 10 ml sample volume to 1.7% for a 250 ml sample volume, and an efficiency of 2.9% for 100 ml for the 3/8-inch crystal. This resulted in a 36 % reduction for a sample volume of 100 ml. The reduced efficiency was due to self-attenuation of the photons in the sample as well as photon emissions from upper layers of the solution emitted in the direction of the detector falling outside the ROI. The one-inch crystal ranged from 8.8% for a 10 ml urine sample to 3.4% for a 250 ml sample, with 5.6% at 100 ml. This resulted in a 33.3% reduction for a sample volume of 100 ml. The difference in efficiency between the two crystals for the 100 ml sample is due to the higher detection efficiency for the 360 keV photons in the one-inch crystal.

The contribution of counts from a urine sample in ROI 1 to the counts of a sample in ROI 2 was determined for separation distances ranging from 0 cm (ROIs touching) to 19.5 cm (See Figure 22). The contribution ranged from approximately 26.5% for ROIs that are immediately adjacent (touching) to 1.4% at a separation of 19.5 cm for the 3/8-inch crystal. The contribution ranged from approximately 26% for ROIs that are immediately adjacent (touching) to 1% at a separation of 19.5 cm for the one-inch crystal.

[Cesium-137](#)

Figure 29 shows for cesium-137 the time post incident that a committed dose of 20 mSv is detectable in urine specimens counted on the Hawkeye gamma camera is approximately 2 days for Type F, and is undetectable for Types M and S. For a MDD of 250 mSv, the time post incident that a dose is detectable is 180 days for Type F, 610 days for Type M and I undetectable for Type S. Although the detection efficiency for the gamma camera is much

lower due to the higher energy photons at 662 keV, the background is comparably less so a window established to detect photons with an average of 662 keV can provide sufficient sensitivity to positively detect intakes resulting in a 20 mSv committed dose or less. The MDD was calculated based on a background value of 7.9 counts per second, determined for 364 keV, which is considered conservative based on the background spectrum versus photon energy displayed by the gamma camera software.

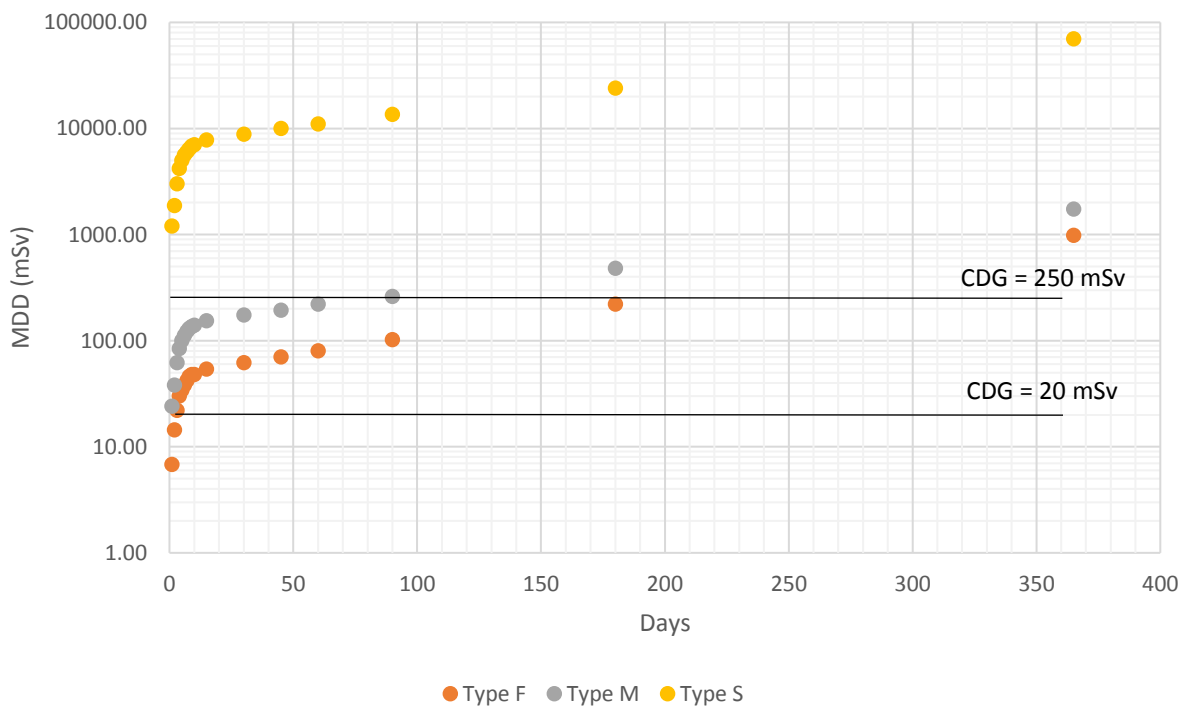


Figure 31: MDD for Cesium-137 (Type F, S, M) days post incident

The detector efficiency as a function of urine sample volume containing Cesium-137 (see Table 11) assuming a constant concentration ranged from 2.2% for 10 ml sample volume to 0.8% for a 250 ml sample volume, and an efficiency of 1.4% for 100 ml for the 3/8-inch crystal. This resulted in a 35 % reduction for a sample volume of 100 ml. The reduced efficiency was due to self-attenuation of the photons in the sample as well as photon emissions from upper

layers of the solution emitted in the direction of the detector falling outside the ROI. The one-inch crystal ranged from 5.2% for a 10 ml urine sample to 2% for a 250 ml sample, with 3.4% at 100 ml. This resulted in a 35% reduction for a sample volume of 100 ml. The difference in efficiency between the two crystals for the 100 ml sample is due to the higher detection efficiency for the 661 keV photons in the one-inch crystal.

The contribution of counts from a urine sample in ROI 1 to the counts of a sample in ROI 2 was determined for separation distances ranging from 0 cm (ROIs touching) to 19.5 cm (See Figure 23). The contribution ranged from approximately 28.3% for ROIs that are immediately adjacent (touching) to 1.9% at a separation of 19.5 cm for the 3/8-inch crystal. The contribution ranged from approximately 28.8% for ROIs that are immediately adjacent (touching) to 1.5% at a separation of 19.5 cm for the one-inch crystal.

[Iridium-192](#)

Figure 30 shows for iridium-192 the time post incident that a committed dose of 20 mSv is detectable in urine specimens counted on the Hawkeye gamma camera is approximately 20 days for Type F, one day for Type M, and is not detectable for Type S. For a MDD of 250 mSv, the time post incident that a dose is detectable is 90 days for Type F, 45 days for Type M and one day for Type S.

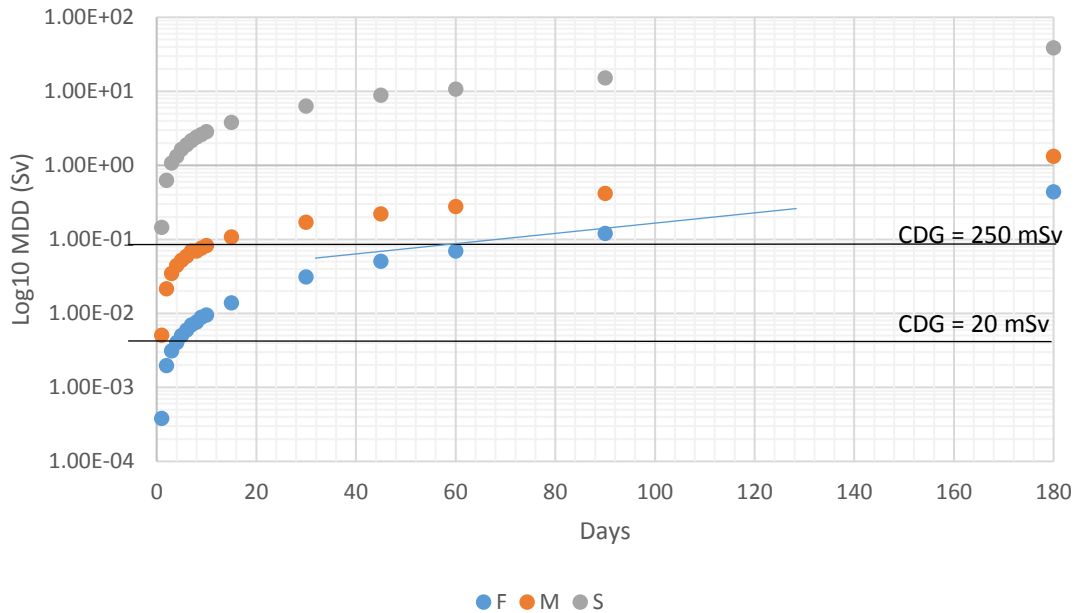


Figure 32: MDD for Iridium-192 (Type F, S, M) days post incident

The detector efficiency as a function of urine sample volume containing Iridium-192 (see Table 11) assuming a constant concentration ranged from 4.9% for 10 ml sample volume to 1.9% for a 250 ml sample volume, and an efficiency of 3.1% for 100 ml for the 3/8-inch crystal. This resulted in a 37 % reduction for a sample volume of 100 ml. The reduced efficiency was due to self-attenuation of the photons in the sample as well as photon emissions from upper layers of the solution emitted in the direction of the detector falling outside the ROI. The one-inch crystal ranged from 8.4% for a 10 ml urine sample to 3.3% for a 250 ml sample, with 5.5% at 100 ml. This resulted in a 35% reduction for a sample volume of 100 ml. The difference in efficiency between the two crystals for the 100 ml sample is due to the higher detection efficiency for the 308 keV photons in the one-inch crystal.

The contribution of counts from a urine sample in ROI 1 to the counts of a sample in ROI 2 was determined for separation distances ranging from 0 cm (ROIs touching) to 19.5 cm (See

Figure 25). The contribution ranged from approximately 26.7% for ROIs that are immediately adjacent (touching) to 1.3% at a separation of 19.5 cm for the 3/8-inch crystal. The contribution ranged from approximately 22.7% for ROIs that are immediately adjacent (touching) to 0.8% at a separation of 19.5 cm for the one-inch crystal.

Volume Throughput

In the event of an incident, the number of urine specimens that could be analyzed using the method in this dissertation is estimated as follows.

The detector dimensions are 60 x 40 cm. An array of twenty-four 10 x 10 cm regions of interest can be assembled on the detector surface and can be analyzed in a single 3-minute count. Assuming a tray of 24 urine specimen containers can be placed on the detector, analyzed, and replaced every 10 minutes, a total of 144 samples can be analyzed per hour. Technologists could, therefore, theoretically analyze a total of 1,152 samples in a single 8-hour shift using a single gamma camera.

This arrangement of sample containers on the detector surface will result in photons emitted from one sample being attributed to the sample in the adjacent ROI. The crosstalk between adjacent (touching) ROIs was consistent at 26% \pm 3%. The impact of this scenario is discussed.

A sample containing significant activity is detected by the gamma camera detector. The samples immediately adjacent to the sample also exhibit activity but at a much lower activity. The adjacent samples, therefore, may or may not possess activity. The central sample exhibiting the highest count should be removed from the tray and the remaining samples counted once again.

Samples containing a higher volume of urine will see a commensurate reduction in detector efficiency depending on photon energy. However, smaller volumes of urine containing low activities may be missed because the gross activity is low. Therefore, the selected volume of 100 ml for a urine sample is a compromise for the tradeoff between sample volume and detector efficiency.

V. Limitations

The MDD is based on several limiting variables. A description of the limitations follows. The urine specimen container used for the sample geometry used in this study is only one of many available. The detection efficiency is related to the cylindrical volume of the container and the quantity of medium. As the height of the cylinder increases, the decays occurring in the upper portion of the column height have a lower probability of being detected due to attenuation in the medium and the increase in distance from the detector surface. Since a region of interest (ROI) of 10 cm x 10 cm was selected, any decays that result in the photon interacting with the detector outside the ROI will not contribute to the sample count. Measurements of the number of counts that are detected was modeled in MCNP as a function of height of the medium in the sample container geometry and increasing area of the ROI and the concentration of radionuclide held constant. The detection efficiency was found to be a function of photon energy, height of liquid in the column and the area of the ROI. A higher efficiency could be obtained if a larger ROI was selected, but this reduces the number of sample containers that could be counted at the same time. For these reasons, a ROI of 10 cm x 10 cm, and a sample volume of 100 ml in the specific model of sterile urine

specimen container provided the optimal counting efficiency while maintaining the capability for high throughput bioanalyses.

The Hawkeye gamma camera was the camera available at the hospital where this research was conducted. There are many gamma cameras available that may offer improved counting efficiency, detector size, and counting geometry. The parameters that were critical to proper modeling of the counting geometry for input to the MCNP model included the thickness of the plastic cover inserted over the detector, the measurement of the air gap between the plastic cover and the surface of the detector. These values were measured using a handheld scale. Inaccuracies in these measurements would lead to differences between measured and modeled detection efficiencies which may be the reason for the 8% difference in measured versus modeled detection efficiency for Tc-99m. However, this difference was considered adequate for validation of the model, and the MCNP derived values of detection efficiencies were then used in the determination of radionuclide specific MDDs.

The MDD is based on the number of counts that comprise background radiation in which the environment the camera is located. During the measurements of background for various energy windows it was noted that radioactivity injected into patients in nearby rooms altered the background values measured. This results in the removal of two data points from background determinations. More background measurements for averaging purposes would have been helpful but the gamma camera was actively used for clinical purposes and impacting patient care was not an option. Additionally, use of the clinical equipment required the presence of nuclear medicine staff which also limited the availability of time of use. However, the spectrum of background radiation was available as a display and was used to

verify the background count rates and conditions. The highest energy that could be measured using available radioisotope settings on the Hawkeye was that for Iodine-131 or 364 keV. It is possible to allow higher energies to be measured on the Hawkeye but would have required reconfiguring the software. This was not done. Instead, the background value measured for the 364 keV \pm 10% window was used for the radioisotopes that produce photons greater than that for Iodine-131. The background spectrum supported this approach and was considered conservative as the number of background counts were lower for higher energy photons.

It is also possible to establish 4 energy windows for a single sample count on the Hawkeye. It is therefore possible to select multiple photon energy windows for a sample count that would increase detection efficiency. However, for the purpose of this dissertation a single energy peak for the predominant photon was selected.

The use of 100 ml of urine in the sample counting geometry is another limitation. The ICRP method used to calculate intake and subsequently, dose, is based on a 24-hour void normalized to a reference person volume of 1.4 liters of urinary excretion per day. The use of smaller samples is allowed in the ICRP method provided the volume correction is made as this is what the intake dose coefficients were based. If smaller volumes are collected for analysis they recommend that the sample be the first void of the day.

The error in the dose coefficients is a limitation in the estimation of intake. The ICRP models are based on studies on animal and human measurements. As such, the results are averaged and are used to represent a single individual. For some radioisotopes such as Iodine-131, the human biokinetic model is very well known as this radioisotope has been used clinically in the treatment of thyroid conditions for several decades. Data for the other radioisotopes used

in this dissertation are also fairly well known as they are available in the nuclear industry and human contaminations have occurred.

VI. Conclusions

This study has shown that the Hawkeye gamma camera can be used to measure radioactivity in urine specimens for the estimation of intake values and subsequent committed effective dose for Type F and M photon emitting radioisotopes with sufficient accuracy to meet dose-based detection limits of 20 and 250 mSv.

Additionally, the use of the gamma camera allows multiple samples to be analyzed at the same time thus allowing large number of samples to be analyzed in a relatively short amount of time. In the event of a large scale incident involving the release of radioisotopes, the gamma camera can be used effectively to screen large numbers of individuals in a population to identify those with an intake of clinical significance. In addition, the use of the gamma camera in a hospital setting addresses CLIA concerns that biological samples be analyzed in an appropriate environment.

Although MDD is a function of detector efficiency, and detector efficiency is affected by sample volume, the selected volume of 100 ml appears to be a logical compromise between the total activity in a sample that can be detected, and the loss in signal due to self-attenuation by the sample media.

Using an array of 24 samples for simultaneous counting may result in additional samples being incorrectly identified as containing activity when they do not, the presence of a sample with high activity can be removed and the remaining samples recounted.

If a 1-inch (2.54 cm) thick NaI crystal gamma camera is used, the detection efficiency is increased for all radionuclides of interest, and lower limits of detection and MDD are possible.

In conclusion, the use of the gamma camera for radiobioassay of urine specimens is sufficiently sensitive to detect intakes below the dose-based clinical decision guidelines provided samples are collected early after the suspected intake. Gamma cameras are a standard device used in nuclear medicine departments throughout the world, are operated by trained staff and in a CLIA setting. The use of the gamma camera for high volume throughput radiobioassay is also it was estimated that 1,152 urine samples could be analyzed in an 8-hour shift, and three times this number if operated continuously over a 24-hour period.

VII. References

- Ahearn, J. F. (1979). *US Nuclear Regulatory Commission 1979 Annual Report (NUREG-0690)*. US Nuclear Regulatory Commission. Washington, D.C.: Government Printing Office.
- Anigstein, R., Olsher, R., & Loomis, D. (2010). *Using Gamma Cameras to Assess Internal Contamination from Intakes of Radioisotopes*. URL: <https://emergency.cdc.gov/radiation/clinicians/evaluation/pdf/instructions.pdf>.
- Ansari, A., & Caspary, K. (2015). *A Guide to Operating Public Shelters in a Radiation Emergency*. Center for Disease Control URL: <https://emergency.cdc.gov/radiation/pdf/operating-public-shelters.pdf>.
- Bailey, M. B., Etherington, G., Fraser, G., & Wilkins, B. (2010). *Individual Monitoring Conducted by the Health Protection Agency in the London Polonium-210 Incident*. Oxfordshire: Health Protection Agency.
- Barnett, D., Parker, C., Blodgett, D., Wierzba, R., & Links, J. (2006). Understanding Radiologic and Nuclear Terrorism as Public Health Threats: Preparedness and Response Perspectives. *Journal of Nuclear Medicine*, 1653-1661.
- Battist, L., & Peterson Jr., H. (1979). *Radiological Consequences of the Three Mile Island Accident*. Office of Standards Development. USNRC.

- Bevelacqua, J. (2005). Internal Dosimetry Primer. *Radiation Protection Management*, 22(5), 7-16.
- CDC. (2014). *Population Monitoring in Radiation Emergencies*. U.S. Department of Health and Human Services, Radiation Studies Branch. Government Printing Office.
- Chilton, A., Shultis, J., & Faw, R. (1984). *Principles of Radiation Shielding*. Prentice-Hall, Inc.
- Christodouleas, J., Forrest, R., Ainsley, C., Tochner, Z., Hahn, S., & Glatstein, E. (2011). Short-Term and Long-Term Health Risks of Nuclear Power Plant Accidents. *The New England Journal of Medicine*, 364(24), 2334-2341.
- Coeytaux, K., Bey, E., Christensen, D., Glassman, E., Murdock, B., & Doucet, C. (2015). Reported Radiation Overexposure Accidents Worldwide, 1980-2013: A Systematic Review. *PLOS One*, 1-26.
- Currie, L. (1968). Limits for Qualitative and Quantitative Determination: Application to Radiochemistry. *Annals of Chemistry*, 40, 586-593.
- Dominguez-Gadea, L., & Cerezo, L. (2011). Decontamination of radioisotopes. *Reports of Practical Oncology and Radiotherapy*, 16, 147-152.
- EPA. (2017). *Protective Action Guides and Planning Guidance for Radiological Incidents (EPA-400/R-17/001)*. Government Printing Office.
- GE. (2012). *Molecular Imaging: Nuclear Medicine Technical Education*.
- Guntay, S., Powers, D., & Devell, L. (1996). *The Chernobyl Reactor Accident Source Term: Development of a Consensus View*.
- Harrison, J., Fell, T., Leggett, R., Lloyd, D., Puncher, M., & Youngman, M. (2017). The polonium-210 poisoning of Mr Alexander Litvinenko. *Journal of Radiological Protection*, 37(1).
- Hine, G. (1967). *Instrumentation in Nuclear Medicine, Vol 1*. New York: Academic Press.
- IAEA. (1988). *The Radiological Accident in Goiania (STI/PUB/815)*. IAEA.
- IAEA. (2004). *Safety Reports Series No. 37 - Methods for Assessing Occupational Radiation Doses Due to Intakes of Radionuclides*. IAEA.
- ICRP. (2007). ICRP Publication 103: The 2007 Recommendations of the International Commission on Radiological Protection. (C. Clements, Ed.) *Annals of the ICRP*, 37(2-4), 1-334.
- ICRP. (2007). *ICRP Publication 107: Nuclear Decay Data for Dosimetric Calculations*. ICRP.
- ICRP. (2015). Occupational Intakes of Radionuclides: Part 1. ICRP Publication 130. (C. Clement, Ed.) *Annals of the ICRP*, 44(2), 1-188.
- ICRP. (2015). *Occupational Intakes of Radionuclides: Part 1. ICRP Publication 130*. Sage.
- ICRP. (2016). Occupational Intakes of Radionuclides: Part 2. ICRP Publication 134. (C. Clements, Ed.) *Annals of the ICRP*, 45(3/4), 1-352.

- ICRP. (2017). Occupational Intakes of Radionuclides: Part 3. ICRP Publication 137. (C. Clements, Ed.) *Annals of the ICRP*, 46(4/4), 1-487.
- Koenig, K., Goans, R., Hatchett, R., Mettler, F., Schumacher, T., Noji, E., & Jarrett, D. (2005). Medical Treatment of Radiological Casualties: Current Concepts. *Annals of Emergency Medicine*, 45, 643-652.
- LANL. (2017). *MCNP6.2 Users Manual*. LANL.
- Miller, C., Whitcomb, R., Ansari, A., C, M., Guinn, A., & Tucker, F. (2007). The Roles of Medical Health Physicists in a Medical Radiation Emergency. *Operational Radiation Safety*, S187-S190.
- Nations, U. (2000). *Sources and Effects of Ionizing Radiation, Vol. II Effects, Exposure and effects of the Chernobyl accident*. United Nations.
- NCRP. (2001). *NCRP Report No. 138, Management of Terrorist Events Involving Radioactive Material*. Maryland.
- NCRP. (2013). *NCRP Report No. 161: Management of Persons Contaminated with Radionuclides*.
- Nomura, S., Tsubokura, M., Gilmour, S., Hayano, R., Watanabe, Y., Kami, M., . . . Oikawa, T. (2015). An evaluation of early countermeasures to reduce the risk of internal radiation exposure after the Fukushima nuclear incident in Japan. *Health Policy and Planning*, 31, 425-433.
- Samet, J. M., & Chanson, D. (2015). *Fukushima Daiichi Power Plant Disaster: How many people were affected? 2015 Report*.
- Tsubokura, M., Nihei, M., Sato, K., & Masaki, S. (2013). Measurement of Internal Radiation Exposure Among Decontamination Workers in Villages near the Crippled Fukushima Daiichi Nuclear Power Plant. *Health Physics*, 105(4), 379-381.
- UNSCEAR. (2008). *Sources and Effects of Ionizing Radiation, Vol. II, Scientific Annexes C, D and E*. New York: United Nations.
- UNSCEAR. (2013). *Sources and Effects of Ionizing Radiation, Volume I Scientific Annex A*. New York : United Nations .